Defence Research and Development Canada | Recherche et développement pour la défense Canada

DEFENCE **R&D** DÉFENSE

Image processing technique for automatic detection of satellite streaks

M. P. Lévesque
S. Buteau
DRDC Valcartier

Canada

Image processing technique for automatic detection of satellite streaks

M. P. Lévesque
S. Buteau
DRDC Valcartier

Defence R&D Canada - Valcartier

Authors

Martin P. Lévesque   &   Sylvie Buteau

Approved by

Jean-Marc Garneau
Section Head, Optronic Surveillance

Approved for release by

Christian Carrier
Chief Scientist

Abstract

This report presents an image processing technique to detect satellite streaks. This method is particularly useful in the context of surveillance of space where the positions of active satellites and other orbital debris must be monitored. In such cases, the orbital parameters are known, but after a certain time this knowledge deteriorates because of the recent orbit perturbations. Consequently, the satellites need to be re-observed and the orbital parameters must be updated before these satellites are declared lost.

Hence, even before its reacquisition, the satellite's motion is known but its position is estimated with a certain margin of error. This knowledge allows for automatic pointing of the telescope, acquiring of images with the satellite streak within the field of view, developing a matched filter (with the motion knowledge) for detecting this streak within the image and declaring of the satellite position.

This study begins with a detailed analysis of a typical image, which includes several sensor artefacts (such as dead pixels, background gradient, noise) and signal degradation (bleeding, blooming, saturation, etc.). This study explains how sensor artefacts are corrected, image background is removed and noise is partially erased. Then, it describes a technique to detect and erase stars. This reduces the number of objects in the image that could generate false alarms. Finally, this document describes how to design and apply a matched filter used for extracting the satellite streak in images. Examples of processed data are illustrated for each of the processing steps.

Résumé

Ce rapport présente une technique de traitement d'images pour détecter les traces de satellites. Cette méthode est particulièrement utile dans le domaine de la surveillance de l'espace où les positions des satellites actifs et d'autres débris doivent être contrôlées. Dans ces cas, les paramètres orbitaux sont connus, mais après un certain temps cette connaissance se détériore à cause des récentes perturbations orbitales. Conséquemment, les satellites doivent être ré-observés et les paramètres orbitaux mis à jour avant que ces satellites ne soient déclarés perdus.

Ainsi, avant même sa ré-acquisition, le déplacement du satellite est connu mais sa position est évalué avec une certaine marge d'erreur. Cette connaissance permet de pointer automatiquement un télescope, d'acquérir des images avec la trace du satellite dans le champ de vision, de développer un filtre adapté (avec la connaissance du déplacement), de détecter cette trace dans l'image et de déclarer la position du satellite.

Cette étude commence par l'analyse détaillée d'une image typique, laquelle inclut plusieurs artéfacts de capteur (tel que des pixels morts, gradient de fond, bruit) et dégradation du signal (coulage, éblouissement, saturation, etc.). Cette étude explique comment les artéfacts du capteur peuvent être corrigés, le fond de l'image enlevé et le bruit partiellement effacé. Puis, elle décrit une technique pour détecter et effacer les étoiles. Cela réduit le nombre d'objets dans l'image qui pourraient générer des fausses alarmes. Finalement, ce document décrit comment concevoir et appliquer le filtre adapté qui est utilisé pour extraire la trace du satellite de l'image. Des exemples de données traitées sont illustrés pour chacune des étapes du traitement.

This page intentionally left blank.

Executive summary

This report describes an image processing technique used for the automatic detection and extraction of satellite streaks from astronomical images. This methodology has been developed expressly for the processing of images produced by the Surveillance of Space (SofS) Concept Demonstrator (CD), which is comprised of three observatories located at Kingston, Suffield and Valcartier. Since these observatories should produce hundreds of images every week, all the acquisition and data reduction tasks must be automated as much as possible.

The algorithms presented in this document are a first step toward a fully automated data analysis system. They automatically process and remove the sensor's artefacts, reduce the image content by removing irrelevant objects and finally extract the satellite streaks. This last step is possible because the data processing is integrated with the tasking and image acquisition system, which provides a priori information about the target motion and sensor pointing. It only lacks a detection validation step to the system, which will be the object of future work.

These image processing algorithms were implemented within the operating software at the Surveillance of Space Operation Center (SSOC) at DRDC Ottawa, which remotely operates the three observatories. Furthermore, these automatic streak extraction algorithms should also be implemented into the SAPPHIRE data processing facility in the near future.

Sommaire

Ce rapport décrit une technique de traitement d'images pour la détection et l'extraction automatique des traces de satellites dans les images astronomiques. Cette méthodologie a été spécialement développée pour le traitement des images produites par le démonstrateur de concept (CD) de la surveillance de l'espace (SofS), lequel est constitué d'une série de trois observatoires localisés à Kingston, Suffield et Valcartier. Puisque ces observatoires devraient produire des centaines d'images chaque semaine, toutes les tâches d'acquisition et de réduction des données doivent être automatisées dans la mesure du possible.

Les algorithmes présentés dans ce document constituent une première étape vers un système entièrement automatisé d'analyse des données. Ils traitent et enlèvent automatiquement les artéfacts des capteurs, réduisent le contenu des images en supprimant les objets non pertinents et finalement ils en extraient les traces de satellites. Cette dernière étape est redue possible parce que le traitement des données est intégré avec les systèmes de planification des tâches et d'acquisition d'images, lesquels procurent de l'information a priori sur le du mouvement de la cible et du pointage du capteur. Il ne manque plus au système qu'une étape de validation de la détection, laquelle fera l'objet de travaux futurs.

Ces algorithmes de traitement des images ont été implantés dans le logiciel d'opération, au centre d'opération de la surveillance de l'espace à Ottawa, lequel télécommande les trois observatoires. De plus, ces algorithmes d'extraction automatique des traces devraient être implantés dans l'unité de traitement des données de SAPPHIRE dans un proche avenir.

Table of contents

List of figures

List of tables

Acknowledgements

The authors would like to thank Mr. François Rivard, who helped to code and test the algorithms in Matlab first and afterwards in C++ during his summer training period

This page intentionally left blank.

1.   Introduction

In the current state of colonization of near Earth space by satellites, there is an increasing need to know exactly the real status of occupation of this space. Thus, orbital parameters for all objects traveling in this space must be known with a high degree of accuracy, and this knowledge must be periodically updated because this situation is always changing. Atmospheric drag, solar wind, moon and planetary gravitational perturbations, Earth oblateness, etc. are all sources of interference that generate orbital perturbations beyond what the best orbital model can predict. The solution is to periodically observe all the satellites, particularly the debris (because active satellites themselves contribute to maintain the knowledge of their orbital parameters), determine with precision their positions and update their known orbital parameters.

To achieve this mission of Surveillance Of Space (SOS), the Space Surveillance Network (SSN) uses several large telescope and radar stations located all around the world. However, these expensive observation stations do not suffice for the observation needs, with the result that objects are lost (due to not being reacquired in time) every week. At the same time, all the observations do not really require execution by such powerful sensors. In order to help to accomplish the mission, a battery of small and low-cost instruments (almost amateur grade equipment) can be deployed to contribute to the necessary data acquisition tasks. For this purpose, the US has developed the RAVEN stations (Refs. 1 and 2) and Canada also contributes to the SSN with similar stations (Refs. 3 to 6), which were initially called CASTOR (Canadian Automated Small Telescope for Orbital Research) for the prototype and finally rename the SofS/CD for 'Surveillance of Space Concept Demonstrator' for the operational deployed stations.

A CASTOR station (Refs. 3 to 8) is based on a Celestron 14 telescope coupled with a temperature compensating focuser, mounted on a Paramount 1100GT German-Equatorial mount (manufactured by Software Bisque), equipped with an Apogee AP8p 1024x1024 pixel CCD camera. This instrument is located inside a 10'6" dome manufactured by Ash Domes and positioned by a dome control system manufactured by Meridian Controls. Three of these stations are spread (to reduce the risk of having a cloud-covered sky) over the Canadian territory (at Suffield, Alberta, Kingston, Ontario and Valcartier, Québec) and are remotely operated from a common operations room (SOC: Sensor Operation Control) located at DRDC Ottawa.

When the certification tests are completed, these three stations will operate in automatic mode. During the day, the operator will establish the observation program for the following night. He will be helped by a schedule optimization program (also in development). The program will be executed at night. The next day, the operator will check system errors, reprogram the stations and communicate the valid observation to the SSN. This implies that the dome opens, rotates and closes by itself (functions assumed by the Meridian dome controller), the telescope slews to the appropriate position at the right time (functions that can be assumed by the Paramount 1100GT German-Equatorial mount along with the software developed by Software Bisque, i.e., 'The Sky', Automadome, Orchestrate and CCD Soft, etc.) and that the camera acquires the images at the right time (a GPS receiver provides an accurate clock). The whole

cycle takes less than 3 minutes for one satellite. The subsequent (longer) step is to download the image from the CCD camera to the computer. Hence, during good atmospheric conditions, it is foreseen that a single station will have the capability to perform up to 300 observations during a long winter night. The issue lies in analyzing all these images.

There is a need to develop algorithms and software that can automatically detect and report the presence of satellite streaks in the acquired images. The algorithms presented in this document were developed for this purpose. They were tested and since they performed very well, they were incorporated into the remote-operation software at the SOC. They are also efficient regarding processing requirements. The first satellite streak detection software showed that the unused CPU time available in the 3 minute observation cycle was sufficient to complete the analysis task. In this 3 minute cycle, the computer can control the station, analyze the last acquired image and report on the satellite observation.

The image processing technique presented in this document is a collection of algorithms used to detect and classify everything that can be observed in the image, such as stars, satellite streaks and image artefacts. The basic approach consists in using a matched filter to detect the streak. However, since it cannot be detected directly with high efficiency, the applied technique consists in detecting anything that can be identified as non-streak (based on morphological characteristics) and then in removing it from the image, leaving a simpler image where the streak is easier to detect. This process reduces the probability of false alarms and increases the sensitivity of the entire algorithm system.

This report begins with an analysis of a typical image where signal components are characterized. Next, special algorithms, for the extraction of each one of these components, are described. One by one, all the non-streak components (in order: sensor artefacts, background, noise and finally the stars) are eliminated from the image before the streak detection algorithm is applied to the remaining signal. All previous algorithms were designed to preserve streaks, i.e., if in doubt, the processing scheme leaves the signal intact to avoid altering streaks, even though the output signal may still contain non-erased stars.

This report describes several inter-dependent ad-hoc algorithms. These algorithms are inter-dependent in the sense that some of them are specifically designed not to inhibit the action of the next processing steps. In other words, they were optimized on the basis of fine trade-offs between the different processing steps rather than through an independent step-optimization procedure that would not take into consideration the negative impacts due to algorithm interactions. For instance, a star erasing algorithm with a lower threshold would be more efficient for star removal but it would also erase faint streaks. In such a case, it is preferable to tolerate a few faint stars (which are tolerated by the next processing step) and preserve the faint streaks. Globally, the algorithms presented in this report are individually sub-optimal and consequently could certainly be further optimized in the near future. Nevertheless, it is shown that their efficiency and performance were adequate to the current application.

It would be interesting to compare the performance of the algorithms developed in this report with other known methods. Unfortunately, there are almost no publications on this subject in the open literature. This is probably because the images were always examined by human observers and the conception of fully automated (operation and data processing) is only a recent requirement. One may think that detecting artificial satellites and asteroids (currently done by astronomers) are similar process, but unfortunately the data acquisition constraints are different and the characteristics of generated data are not equivalent. For artificial satellite detection, only one paper deserved to be mentioned. This paper by Sanders-Reed (Ref. 9) describes a maximum likelihood filter technique based on an accurate noise model. Although the maximum likelihood filter is certainly better at detecting other 'unexpected' satellites, a matched filter technique was favoured in the current approach because of its higher sensitivity for the 'expected' satellites.

The detection method developed in this report is implemented in the SOC and has been tested with hundreds of images. It has proven to be very stable and sensitive. The results showed that it is able to detect streaks with a signal-to-noise ratio above two. The exact figures of merit are not evaluated yet.

At the moment this report is being published, the detection algorithms are being refined (for an higher sensitivity) with the addition of a post-detection false-alarm rejection algorithm and the production of these figures of merit has begun. This will be published in Ref. 10.

This work was performed between September 2004 and February 2005 under the project 15et13: 'Small telescope for Surveillance of Space'.

2.   Image characterization and correction

The first step in the development of an image-processing algorithm is to analyze typical images in order to characterize all signal components. For this purpose, let us begin with a typical case such as the one below.

Figure 1 shows a typical image acquired with the CASTOR system. In the middle of the image, there is a very small and faint satellite streak. By inspecting the digital image along with contrast manipulation software, a trained user will detect it without difficulty. However, the system is designed to acquire hundreds of images per clear night and fatigue could become a factor that would limit the operator's performance. Therefore, there is a serious need for an algorithm that can automate the detection process, i.e., read the acquired image and generate a formatted report, which could be used as an input by another program. This report could contain the coordinates of the streak end-points along with a very accurate time of reference and the astronomical positions.
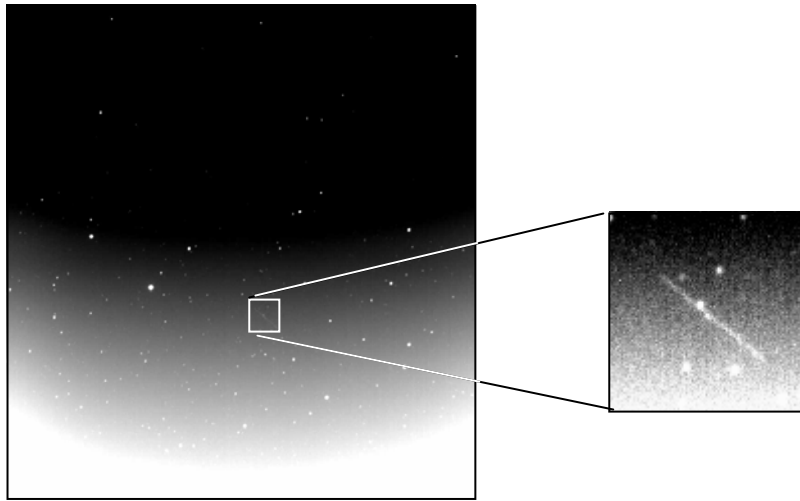
Figure 1. Typical image, acquired with amateur-grade telescope and CCD, that contains a faint satellite streak

The goal of the processing method presented below is to extract such a very faint signal almost lost in the noise, among sensor artefacts and strong signals of bright stars. It is mandatory to carefully analyze images, identify signals and artefacts and make a good image characterization. Once this is done, one can note that these image components are separable and can be removed. After removing these "extraneous" image components (bright stars, sensor artefacts), the faint satellite streak, almost lost in the original image, becomes more readily visible. The processing begins with identifying each of the potential sources of trouble and with finding an adequate solution to each one of them. In the following sections, all the image artefacts, which are taken into account in the whole process, are presented. Some of them are obvious and do not really need detailed descriptions. Others are more complex and require special attention.

2.1 Camera artefacts

The first noticeable image artefact (Fig. 19-B1) is the gradient of the image background. This artefact is very important and requires special attention but it does not really represent a big challenge. This subject will be described in detail later.

The second important image artefacts are the detector's bad pixels. This problem has a very classical solution, which consists in interpolating the known bad pixels using the values of its neighbours. This method only requires building a list of bad pixels (or line segments), which is specific to each CCD camera but common to all images acquired by the same CCD.

Another apparent acquisition artefact is the dark window border effect. Very often, the last image lines and columns (sometimes up to 20 consecutive lines) are very dark. After analysis, it seems that the gain factor is incorrect for these lines. This image artefact is compensated by using a polynomial fit on the image background (the same method described below for the background removal method) and by checking whether the last lines (and columns) have average values lower than expected. For these image lines, the gain is readjusted and the border artefact disappears. The elimination of this dark window effect makes the signal more homogeneous and prevents further difficulties for the next processing steps.

2.2 Image noise

Finally, the last sensor artefact and not the least is the noise, principally generated at the acquisition by the CCD dark-current noise (almost Gaussian), the readout system and partially by the photon noise (Poisson noise). When evaluating the image background, the CCD noise is dominant (at least for the amateur-grade CCD that was used). This noise directly depends on the sensor temperature. With the limited performance of the cryo-cooler install on the camera, very often the CCD is not cooled enough. Furthermore, the noise statistics are not constant in the image. The noise is at its lowest values in the top of the image where the pixels are the first to be read by the ADC (analog to digital converter). The noise level gradually increases toward the bottom of the image (Fig. 19-B2), varying from the simple to the double. This indicates that there are cumulative effects due to the CCD readout mechanism. Therefore, the local noise is always a factor under consideration in the filter design presented below. It is used as the determining criteria to establish the limit of sensitivity for the local filters. For this purpose, the standard deviation is calculated assuming Gaussian noise (such as shown in Fig. 2). This assumption is not exact but it is accurate enough for the current application.

However, from time to time, single pixels (or pairs of pixels) have brightness far above the Gaussian distribution (typically $10\sigma_n$ to $20\sigma_n$). The origin of these noise spikes has not yet been investigated. They are not necessarily caused by hot pixels (bad pixels with an excessively high gain) because they do not occur systematically at the same locations in every image. They may simply result from a combination of several noise sources with different distributions. It is certain that their occurrence has a very negative influence on [local] noise estimation and on the star detection algorithms. However,

they are very easy to detect and eliminate. When detected, they are set to zero (or at least to the local signal average if the image background has not yet been removed) and the remaining image background is easily processed as if the remaining noise was truly Gaussian.

	A: Background noise: (almost Gaussian) Image: signal clipped to $\pm 2\sigma_n$.	
	B: Noise spikes: Image: signal clipped above $3\sigma_n$. Spikes are single pixel with exceptional brightness far above main distribution ($\gg 3\sigma_n$) and they are easily identified and removed.	
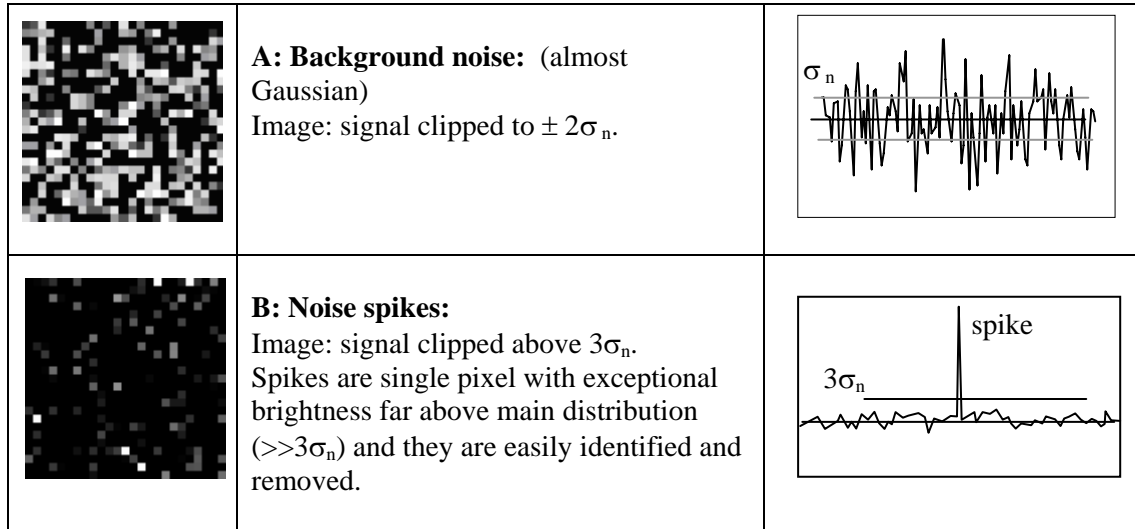
Figure 2. Gaussian-like noise and noise spikes

2.3 Signal dependent artefacts

The next category of artefacts depends on the sensor response to the signal itself. The signal saturation is an expected phenomenon. On the other hand, the blooming and bleeding are less expected and must be carefully examined to evaluate their impacts on the performance of the streak detection algorithm. Figure 3 illustrates what happens to the signal properties when different star brightnesses are encountered.

For a bright star (see Figure 3) that is well above the noise level but still far from the saturation level, the optical impulse response is clearly visible in the star profile. Typically, this represents a star that covers approximately 10% of the sensor dynamic range. With the optical setup used at the CASTOR stations, i.e., the combination of atmospheric transmission, telescope and CCD, the width of the star profile at half height is around three pixels. This is the star radius that was considered in the filter design. However, for other systems with higher resolution (very often the Nyquist criterion is not applied in astronomical systems) this value should be different.

For fainter stars, the star size remains the same, except that the profile (the PSF, i.e., the Point Spread Function) becomes more irregular due to the sampling effect. For very faint stars, the profile cannot be used but the aggregation of pixels remains visible for object brightnesses only a few sigmas (standard deviation of the noise) above the

background. These last objects can be ignored because they do not represent a limiting factor for the satellite streak detection.

On the opposite end, the very bright stars (see Figure 3) can be a serious source of problems. First, for the streak detection algorithm, they are sources of signal that are in competition with the satellite streak. Therefore they need to be detected first and removed from the image. Second, when the brightness increases, the width of the star profile also increases. This can only be explained by a sensor deficiency; when heavily exposed, the electron charges in the CCD pixels increase to the point that the electrons are repulsed in the neighbour pixels, producing a blooming effect. Thus, the filter designed to detect and remove the stars requires several passes, where each pass is adapted for a specific range of star brightness and size.

Afterwards, when the signal intensity continues to increase, the problem of saturation appears. The streak-processing algorithm can tolerate a few slightly saturated stars. However, a single star with several saturated pixels is an indication of other fatal artefacts. First, the half-height width of the star profile does not increase proportionally with the number of saturated pixels. Hence, it is important to count these saturated pixels. A count above a certain limit is an indication that the image is degraded by severe artefacts (visible diffraction and reflection patterns) and this image should not be process. It should be simply discarded. Second, the aspect ratio of these saturated pixels is an indication of another problem: bleeding. Figure 3 shows a saturated star where the bleeding has just begun to appear (aspect ratio smaller than 2) and a very saturated star with a catastrophic bleeding. Algorithms were developed to erase the bleeding by interpolating the saturated pixels from the nearest valid pixels. However, additional analyses have shown that this interpolation is not useful when severe bleeding is detected (i.e., with a height/width aspect ratio greater than 2 or 3) because the image is useless. As a matter of fact, a strong bleeding is an indicator that the star is so bright that several diffraction patterns appear in the image (halos, secondary and parasitic reflections, etc.). For that case, the image background cannot be removed (because of complex structure of the star pattern) and the satellite streak cannot be detected. Therefore, it is important to program the telescope to avoid acquiring satellite streak in the presence of very bright stars. Prior to processing the image, saturated stars must be counted and if the sum exceeds a determined threshold, the image must be rejected.
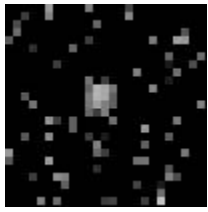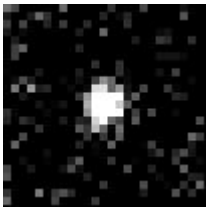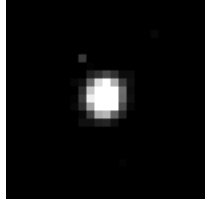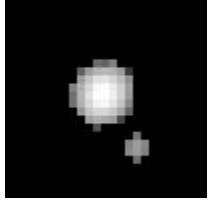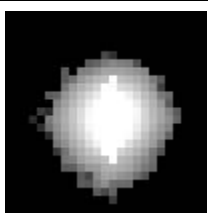
	Very faint stars: $3\sigma_n < \text{SNR} < 10\,\sigma_n$ or typically signal < 0.5% of the sensor dynamic range. Comment: Irregular shape, peak profile visible on 5 to 9 adjacent pixels, effects of the optical impulse response still visible.
	Faint stars: $10\sigma_n < \text{SNR}$ or typically 0.5% to 4% of the sensor dynamic range. Comment: Gaussian profile obvious due to the optical impulse response (along with the atmospheric propagation), star completely contained in a (6x6) window (half-height width = 3 pixels)
	Medium and bright stars: 4% to 15% of the sensor dynamic range. Comment: Clean profile, slightly larger impulse response caused by a light blooming effect. window size = (8x8) pixels to (10x10) pixels
	Very bright stars: 15% to 100% of the sensor dynamic range. Comment: Strong blooming effect visible, requires a larger window size to encircle the star: (13x13) pixels and more. Furthermore, the Gaussian shape of the star has a long decay and its signal is perceptible above the background noise as far as 20 pixels from its center, even if its half-height width is only 7 or 8 pixels
	Saturated stars: Comment: Case by case, local window size depends on the size of the saturated area: - 4 saturated pixels: strong blooming, require at least a 14X14 window - 7 saturated pixels: very strong blooming, requires at least a 25x25 window
	Very Saturated stars: Comment: Gaussian profile severely truncated at the maximum range. Very large area of saturated pixels. Not only the blooming artefact is severe but there are also strong bleeding artefacts. When detected, there is a big chance that the image cannot be used to detect faint satellite streaks because of the other diffraction artefacts (halo) introduced in the image. The image shows Vega with a 10 s exposure with a CCD mounted on a 40 cm Celestron telescope.

Figure 3. Star morphology

2.4   The satellite streaks

After having described everything that we want to get rid off, it remains only the signal we are looking for: the satellite streak. This is the approach used to facilitate the satellite detection. It is difficult to detect streaks but it is quite easy to detect everything else. Hence let us eliminate everything in the image that does not look like a satellite streak until the streak becomes one of the dominant remaining objects.

The following figure illustrates examples of satellite streaks that the algorithm must detect. If streaks were always very bright, a simple intensity threshold would be enough to detect them, but this rarely happens. Since it is desired to detect fainter and fainter objects, the performance of the detection technique must be optimized to detect objects close to the limit imposed by the noise and sensitivity of the observation system. The algorithm presented in this document can detect satellite streaks with average intensities lower than the noise standard deviation.
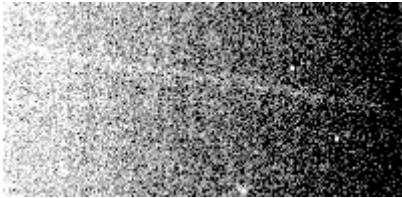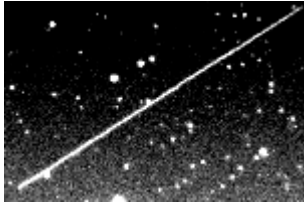
	Usually, the satellite streak is a small line segment, very often almost lost in the noise. Generally, the user must manipulate the image contrast to seen the satellite streak. In this small image, the intensity of this streak is three times the noise standard deviation and less than the background gradient variation (from end to end).
	In this example, the average intensity of the streak is 0.75σ, almost lost in the noise. Due to the great number of pixels in the streak, it is still observable and detectable. However, the noise level prevents determining the end-points.
	This last case illustrates a very clear streak (that rarely happens). It also illustrates the fading effect that frequently occurs with low orbit objects, because of their entry into the Earth limb. Geostationary and Molnyia active objects are usually more constant (for short exposure), except for the debris that often rotates and changes its reflective properties during rotation.

Figure 4. *Examples of satellite streaks*

3.   Processing overview

Now that the image is properly described, it is easier to see that these different objects (noise, background, stars and streak) are separable objects that can be processed individually. Figure 5 illustrates the global processing. The basic idea for detecting difficult streak, as already described previously, is to first remove everything else that can be detected and removed.

To detect an object with a known shape, the maximum sensitivity is achieved with a matched filter. However, the drawback for such a filter is the generation of false alarms by other objects. Particularly, the stars (almost Dirac's delta) produce strong matched-filter responses. Nevertheless, the stars are easy to detect with filters that use local statistics, but such filters are easily eluded by the image background. Fortunately, the background can be easily evaluated and subtracted using polynomial fits. Therefore, the background is removed first, followed by the stars and finally the streak is detected, as illustrated in Figure 5.

Each of these steps requires special attention. When removing the background, small features above the average background (stars, streaks, etc.) must be ignored. Thus, when a pixel signal is too high, comparatively to its neighbours (presence of a star), this pixel is not considered in the polynomial fit used to estimate the background. This is described in Chapter 5. After that, before the stars are detected using local statistics, special attention is given to the noise spikes (in Chapter 6), which are sharp and intense noise events. A spike is electronic noise, and since it is not created by photons propagated through the optics, it does not have the typical optical impulse response profile (PSF). It is narrower, typically only one pixel width. These noise spikes severely reduce the performance of the star detection algorithm. Afterwards, the stars are easily detected but their removal is tricky. Their profiles must be evaluated and subtracted. The details are explained in Chapter 7. Finally, the matched filter is applied to detect the satellite streak. The matched filter response is not as sensitive as desired, but an iterative approach can meet the desired detectability levels. This method is presented in Chapter 8.

```
                    ┌─────────────────┐
                    │   Input image   │
                    └─────────────────┘
                             │
                             ▼
              ┌──────────────────────────────┐
              │ Image correction:            │
              │  -Bad pixel interpolation    │
              │  -Edge recalibration         │
              └──────────────────────────────┘
                             │   Fig. 19A
                             ▼
        ┌──────────────────────────────────────────────┐
        │ Detection of saturated stars:                │
        │  -Build list of saturated stars              │
        │  -Bleeding detection: correction or program  │
        │   interruption if the bleeding is too important │
        └──────────────────────────────────────────────┘
                             │
                             ▼
        ┌────────────────────────────────────┐        ┌──────────────────────────────┐
        │ Model and remove image background  │───────▶│ Output :                     │
        └────────────────────────────────────┘        │  -Image background           │
               │  Fig. 19C   Fig. 19B1 and             │  -Local noise estimation     │
               │             Fig. 19B2                 └──────────────────────────────┘
               ▼
        ┌────────────────────────────────────┐
        │ remove noise spikes                │
        └────────────────────────────────────┘
                             │
                             ▼
   ┌──────────────────────────────────────────────────┐    ┌──────────────────────┐
   │ Remove bright stars:                             │───▶│ Output :             │
   │  -Detect stars using an intensity threshold      │    │ Star map             │
   │  -Get coordinates                                │    └──────────────────────┘
   │  -Measure profile                                │          │  Fig. 19D
   │  -Erase central disk                             │          ▼
   │  -Subtract peripheral crown using modeled profile│      Toward
   └──────────────────────────────────────────────────┘      astrometry
                             │  Fig. 19E                       software
                             ▼                                   │
        ┌────────────────────────────────────┐                  ▼
        │ Remove faint stars using a         │               Fig. 19F
        │ modified double-gate filter        │
        └────────────────────────────────────┘
                             │  Fig. 19G
                             ▼
 ┌──────────────────┐  ┌──────────────────────────────────────┐
 │ Generation of    │  │ Satellite streak detection           │
 │ expected         │  │   ┌────────────────────┐             │
 │ satellite streak │─▶│   │ Matched filter     │ Fig. 19J    │
 └──────────────────┘  │   │ (convolution)      │ Fig. 19L    │
       Fig. 19I        │   └────────────────────┘             │
                       │   ┌────────────────────┐             │
                       │   │ Image clipping     │             │
                       │   └────────────────────┘             │
                       └──────────────────────────────────────┘
                             │  Fig. 19K
                             ▼
        ┌────────────────────────────────────┐
        │ End-point detection                │
        │  - Hough transforms                │
        │  - End-point determination         │
        └────────────────────────────────────┘
```

Figure 5. Processing overview. Images at various processing steps are shown in Fig. 19.

4. Detection of saturated stars and bleeding estimation

This task is essential to evaluate the image quality because when extreme bleeding is detected, the image is probably useless. Therefore, the saturated stars need to be detected and characterized.

The process begins by counting the total number of saturated pixels (an intensity of 65535 for a 16-bit image) in the entire image. Then, starting with a saturated pixel, a region-growing algorithm is applied to gather all the contiguous saturated pixels of the first star. The minimum and maximum coordinates in height and width are recorded and the aspect ratio is estimated. After that, the number of saturated pixels of the first star is subtracted from the total number of saturated pixels and the algorithm searches for the next star until there are no more saturated pixels in the image. The final output of this algorithm is a list of saturated stars, with their position, number of saturated pixels per star and aspect ratio. This list will also be used later for the first estimation the image gradient background, because it indicates non-background pixels.

This approach allows differentiating two cases. The saturated pixels can be distributed into a few severely saturated stars or into several "barely" saturated stars. In both cases, the total number of saturated pixels can be the same. In the first case, each star has several saturated pixels and presents bleeding symptoms. Images of this kind should not be processed; they are useless. For the second case, there are several saturated stars, each one having only a few saturated pixels. These images can be processed correctly. Experiments have shown that the streak detection algorithms performs well with several stars containing no more than 5 to 10 saturated pixels each. However, a single star that has more that 25 saturated pixels (and an aspect ratio height/width above 3 indicates a bleeding effect) is an indication that the CCD is bloomed and that optical artefacts (diffraction, reflection, etc.) will be visible in the image.

5. Background removal

Background removal is a critical step in the current processing. The performance of the star and streak detection algorithms depends on the quality of the background-removal algorithm. The later must not leave any residual background that could corrupt the evaluation of local noise and signal statistics. The local statistics evaluation is based on the assumption that the background is null.

The dark-frame method was first tested. However, two consecutive expositions (with identical condition, even two dark frames) do not really generate identical backgrounds. The image gradient is slightly different from one exposition to another and, when subtracted, they never cancel each other perfectly. Experience showed that this is principally due to cryo-cooler deficiencies. The problem could have been avoided by using better hardware operated in better conditions. It was however decided to operate the cheapest possible hardware (amateur grade) as long as the sensitivity requirement is met. Moreover, the dark frame method doubles the sensor workload, which is not desirable.

Several commercial software products were also tested to remove the image background gradient. Usually, these software packages provide significant image improvements but some image artefacts (residual local background) remain that are not desirable for the streak detection purpose. Therefore, it was decided to develop a specific method for background removal. This method takes into account the characteristics of the sensors used in the system and the application constraints.

This method is based on the fact that the image background is very smooth and can be modeled with polynomial fits. However, the presence of signals (stars and streak) prevents a classical polynomial method from obtaining exact background estimation and the result of a blind fit is inadequate. Thus the method is improved with a few intelligent rules, which consists of an initial estimate for detections of stars that will be ignored in the background estimation. However, to detect a star with its brightness and an intensity threshold, the algorithm needs to evaluate the background, which does not seems make sense since the problem is in the answer. This problem is solved with an iterative process such as shown in Fig. 6. Therefore, a first blind iteration is done where the polynomial is fit the image which includes the stars. Using this first preliminary background estimation, a second polynomial fit is calculated where all objects brighter than the previously estimated background are truncated in intensity (using a rough threshold), producing a better estimation. Finally, this same operation is repeated a third time with a threshold that is well adjusted to the background. This third estimation truncates every star to produce estimation satisfactory for our purposes.
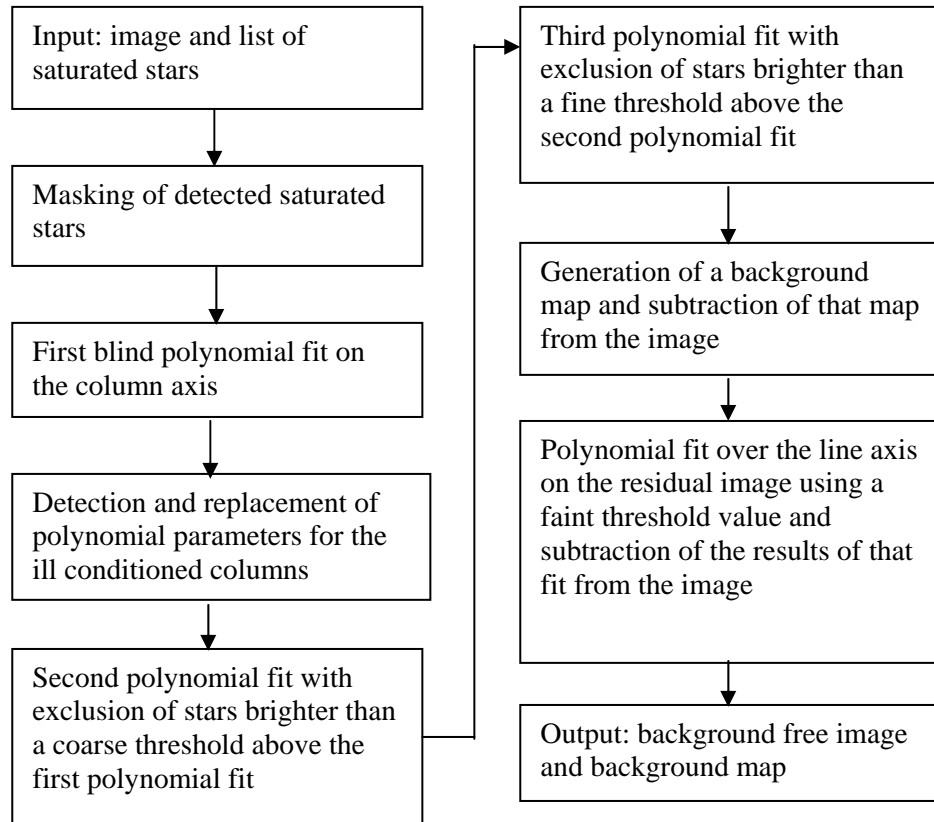
```
┌─────────────────────────┐        ┌─────────────────────────┐
│ Input: image and list of│        │ Third polynomial fit with│
│ saturated stars         │        │ exclusion of stars brighter than│
└─────────────────────────┘        │ a fine threshold above the│
             │              ┌──────▶│ second polynomial fit   │
             ▼              │       └─────────────────────────┘
┌─────────────────────────┐ │                   │
│ Masking of detected     │ │                   ▼
│ saturated stars         │ │      ┌─────────────────────────┐
└─────────────────────────┘ │      │ Generation of a background│
             │              │      │ map and subtraction of that map│
             ▼              │      │ from the image          │
┌─────────────────────────┐ │      └─────────────────────────┘
│ First blind polynomial  │ │                   │
│ fit on the column axis  │ │                   ▼
└─────────────────────────┘ │      ┌─────────────────────────┐
             │              │      │ Polynomial fit over the line axis│
             ▼              │      │ on the residual image using a│
┌─────────────────────────┐ │      │ faint threshold value and│
│ Detection and replacement│ │      │ subtraction of the results of that│
│ of polynomial parameters │ │      │ fit from the image      │
│ for the ill conditioned  │ │      └─────────────────────────┘
│ columns                  │ │                   │
└─────────────────────────┘ │                   ▼
             │              │      ┌─────────────────────────┐
             ▼              │      │ Output: background free image│
┌─────────────────────────┐ │      │ and background map      │
│ Second polynomial fit    │ │      └─────────────────────────┘
│ with exclusion of stars  │ │
│ brighter than a coarse   │─┘
│ threshold above the first│
│ polynomial fit           │
└─────────────────────────┘
```

Figure 6*. Iterative polynomial fit process to remove the image gradient background*

Before describing the method in detail, it must be mentioned that the image columns are easier to model than the lines (specifically for that CCD camera), as shown by the extracted profiles illustrated in Fig. 7. These profiles illustrate the image background gradient along with star inclusions. One can see that the vertical gradient is basically a 'ramp' function, which is probably an artefact created by an accumulation of bias electrons in the analog to digital converter (ADC) in the CCD shift register mechanism. One can also see that a first order polynomial can easily fit that background. Moreover, a careful analysis shows a small third order component that should be taken into account. The line profiles appear to be second-order curves with potentially higher order components that appear harder to model. Therefore, it was decided to model the background with polynomials fitted on the column axis.
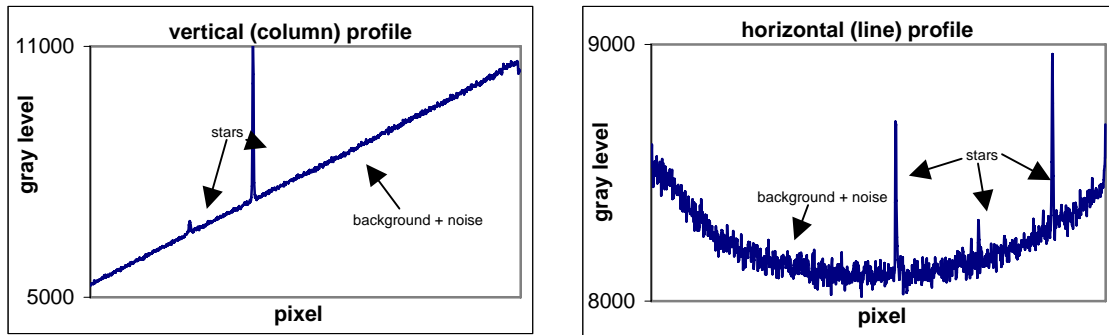
Figure 7. *The column and line profiles extracted from the image indicate that the background is by far easier to model over the column axis*

As written above, the first iteration is performed without clipping the stars, except for the already known saturated stars (as detected in the previous section). The areas surrounding these saturated stars are ignored in the 'first' background estimation. The sizes of these areas are discussed below in Section 7 'Star removal'. A series of first polynomial fits of the third order are then calculated over the 'jth' columns, resulting in a rough 'first' background estimation (pixel (i, j) = $P_{0j} + P_{1j} i + P_{2j} i^2 + P_{3j} i^3$). After correction with this 'first' estimation (explained in next paragraph), a 'second' improved background estimation is obtained by ignoring all bright stars. This time, the bright stars are simply truncated by applying a coarse threshold value, which is equal to the previous background estimation plus 2% to 5% of the sensor dynamic range. This produces a 'second' background estimation with an error of only a few counts per pixel. This process is repeated again a third time with a finer threshold. The noise level (σ_n) is evaluated and the fine threshold is set to 3 σ_n above the 'second' estimated background. This time we almost obtain a perfect 'third' background estimation.

Faint horizontal bright bands may remain at this step. They are created by the inability of a third order polynomial to exactly model the background. Using a higher order for the polynomial only causes a change in the pattern of these horizontal bands. The polynomial fit generates a 'bouncing' effect in the image. This artefact is eliminated by using the same polynomial fit again over the line axis rather than the column axis. Also, one must note that the last pixels in lines or columns are never considered in the polynomial fit method because of the dark edge frame artefact described above.

As mentioned previously, the first polynomial fit requires special attention. This first background estimation contains ill-conditioned column fits, due to the presence of very bright stars that strongly influence the results. If they are not taken into account immediately, the convergence of the method is severely reduced and may require several additional iterations before the background is correctly removed. However, there exists a quick way to immediately locate columns that contributed to bad fit results. The polynomial coefficients of every column polynomial fit are compared and, since the background is relatively smooth, coefficients of neighbouring columns should be very similar. If not, the differences indicate that some fits are corrupted, as shown in Fig. 8.

In those cases, the wrong coefficients are replaced by values interpolated from their neighbours. These 'outlaw' values (in blue in Figure 8) are simply detected with a low order polynomial fit calculated over all the equivalent coefficients (e.g. over the coefficients P_0 of every fit performed for every image column). Then, the standard deviation between the coefficients and the result of that fit is evaluated. Finally, the coefficients whose values differ by more than 3σ, relatively from the main sequence (indicated in blue in Fig. 8), are replaced by interpolated values. Lower differences (in red in Figure 8) are not compensated because they likely represent non-homogeneity in the CCD channel reading mechanism (each image column represent a different channel), and it is a desired effect that the background removal algorithm also removes this artefact. This process of coefficient comparison needs to be done only for the first iteration. Afterwards, the background removal algorithm converges very rapidly.
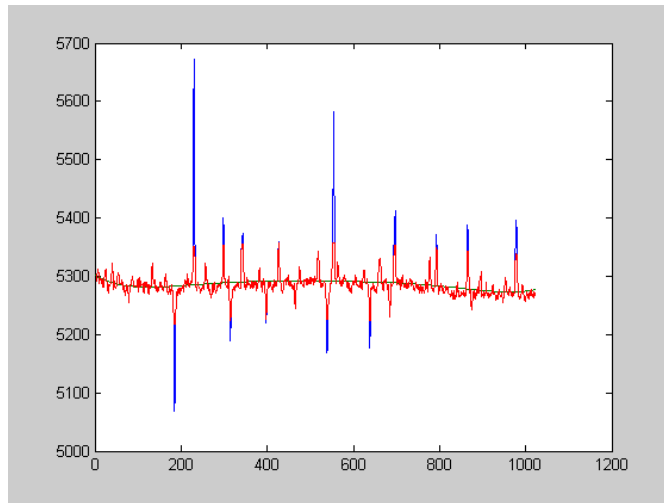
Figure 8. *This graph shows the results for coefficient P_0 (but the graphs are similar also for P_1, P_2 and P_4) after the first iteration. The polynomials were calculated over each of the 1024 image columns. Since the background is very smooth, the coefficients should be approximately the same for all image columns. The blue spikes indicate the columns where incorrect coefficients P_0 were calculated because these image columns contain bright stars.*

6.   Noise spike removal

Given that the algorithm for star detection and removal is based on a local estimation of the noise and signal, it is very important that the noise itself does not include erratic spikes that could be misinterpreted as a real signal. During the execution of the background removal algorithm (Figure 19B1), the noise standard deviation 'σ_n' (Figure 19B2) had been calculated everywhere in the image, except for the areas containing stars. At these locations, the noise characteristics were interpolated. Typically, noise level increases by (almost) a factor two from the top to the bottom of the image for the considered CCD camera. Subsequent noise measurements, with a small window (3x3), produce local estimations σ_{ij}, which are roughly equal to 0.5 to 3 times the known standard deviation σ_n. This variation is normal considering the limited number of pixels (9 pixels) for the estimation.   However, a noise spike may suddenly produce stronger variations, sometimes more than 10 σ_n.

All real objects, except the noise spike, have a width imposed by the optical impulse response (PSF: point spread function). As already shown previously in Figure 3, even the faintest stars are a few pixels wide. Figure 2B shows that this is not true for noise spikes which are created by the electronics. Hence, a simple but efficient filter was designed to detect and remove these bad pixels (spikes) that could generate problems later.

The filter principle consists in erasing the intense objects whose profiles are narrower than the optical PSF. For a PSF with a half-height of 3 pixels, every pixel around the pixel of maximum intensity (of a given star) has at least half the intensity of this pixel. For a noise spike, this relation is not preserved. There is no optical convolution that creates dependence between the pixels.

The filter is shown in Fig. 9. When a pixel 'A' shows an intense signal ($> 3\sigma_n$) and its neighbour pixels ('B', 'C', 'D' or 'E') look like noisy background ($< 2\sigma_n$), then the pixel is reset to zero. This removes 90% of the noise spikes.

However, signal analysis showed that there are often two or three consecutive noise spikes. A real star would generate a two dimension array of pixels. The very faint star presented in Figure 3 has approximately 5x5 pixels and the PSF function is visible on both axes. The image contains several intense objects which are a few pixels long on one axis and only one pixel wide on the other axis. Such an object cannot be created by photons propagated through the optical system.
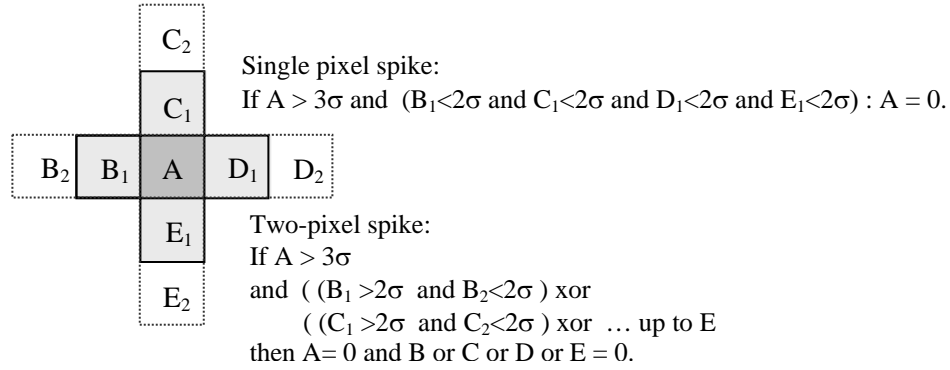
Single pixel spike:
If $A > 3\sigma$ and $(B_1 < 2\sigma$ and $C_1 < 2\sigma$ and $D_1 < 2\sigma$ and $E_1 < 2\sigma) : A = 0$.

Two-pixel spike:
If $A > 3\sigma$
and $(\,(B_1 > 2\sigma$ and $B_2 < 2\sigma\,)$ xor
$(\,(C_1 > 2\sigma$ and $C_2 < 2\sigma\,)$ xor … up to E
then $A = 0$ and B or C or D or E $= 0$.

Figure 9. *Geometry of the kernel used to remove the noise spikes like those illustrated in Fig. 2*

Therefore, a better filter can be conceived by considering the occurrence of consecutive spikes. The second filter, presented in Figure 9, considers that an intense pixel can be a spike if no more than one other adjacent pixel is more intense than the noisy background. When this occurs, both pixels are reset to zero. This filter removes more than 99% of the spikes and considerably improves the performance of the subsequent filtering operations. Considering other geometries of spike occurrence would make for unnecessarily complex algorithms with little or no significant performance improvements.

7.   Star removal

The streak detection algorithm is based on a matched filter technique. This filter readily detects line segment shapes. Its main drawback is the false alarms that might be generated by other objects (like stars). Moreover, bright stars (which have more energy, or counts, in their peaks than a satellite streak has in its whole trace) may generate stronger responses than the sought satellite streak. Therefore, a straightforward solution is to detect and erase the stars prior to make an attempt at detecting satellites.

The stars are easy to detect. The challenge is to detect and erase them without affecting a yet undetected satellite trace. The main difficulty lies in the fact that different stars have different characteristics, as shown in Fig. 3. No single methods can erase all stars in a single pass. Therefore, depending on the star brightness, blooming and spatial distribution, several filtering iterations are performed with filter parameters adapted to a specific class of star.

7.1   Star detection:

Stars are detected and erased in a 3-step process, starting with saturated stars, then with bright stars and finally with faint stars. The saturated stars are already known since they were detected before the background removal process. They are erased using the method described in the next section.

The very bright and faint stars are both detected with adapted double-gate type filters. The local-window geometry of those filter are adapted to the star apparent radius (depending on the blooming). This is why two (if not three) filter passes are required with different window geometry and threshold values. We will describe in the following paragraphs how the detection filter is designed.

Discriminating stars from streaks is simple. All the star pixels are located inside a very small region, whereas the streak pixels (the direction of which has not been not specified yet) cannot be confined in that same region. Hence, using a double-gate filter, it is possible to measure the star signal in the inner window (using the evaluated values of local mean μ_{in}, local standard deviation σ_{in} and the local maximum intensity max_{in}) while the outer window (with μ_{out} and σ_{out}) confirms that there is only "background noise" surrounding the star. Figure 10 shows that this is true only for a single star. This is false for a streak of a significant intensity because there is also a measurable signal in the outer window.

This classical double-gate filter is convenient when the star profile is smaller than the inner window, but this is not always the case. Furthermore, the outer window lacks sensitivity because when it tries to check for the presence of the streak prolongation in the outer window, the local statistics are calculated in the presence of a large area of background, which reduces the filter sensitivity. Therefore, this basic filter is modified and its new design, presented in Fig. 11, proves to be more efficient for streak detection in the outer window.
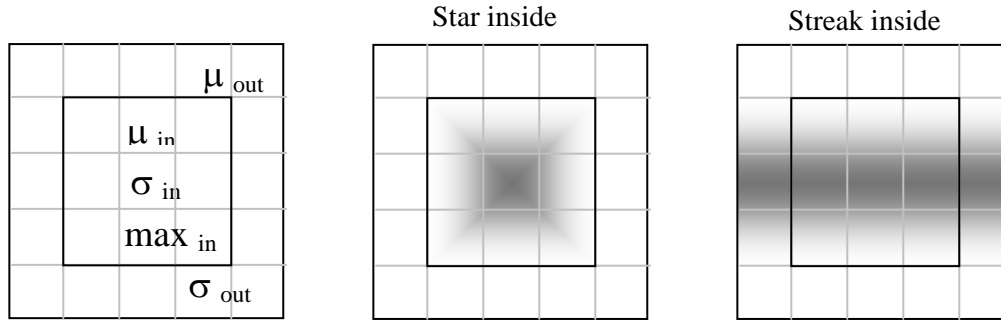
Star inside

Streak inside

Figure 10. *A double-gate filter for star detection where the 9 pixels in the inner window are used to evaluate the star statistics and the 16 outer pixels evaluate the background*
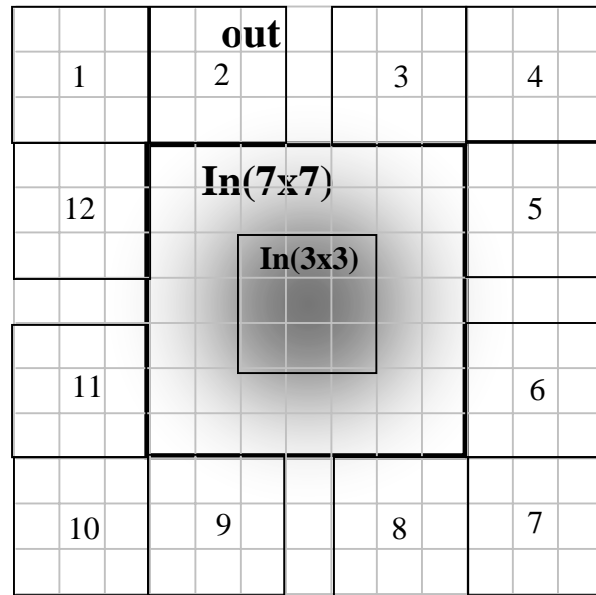

Figure 11. *Multiple-window filter for the detection of faint stars. Inner window is 7x7 pixels for faint stars and could be increases up to 13x13 pixels for bright stars, to correct for blooming effect. The outer windows are used to detect the presence of a streak*

In this new design, a faint star (with a half-height width of 3 pixels) is completely confined inside the inner 7x7 pixel window. Its average value μ_{in} is easy to evaluate over this area. For a more sensitive method, the maximum-intensity pixel could be found (inside that area) and μ_{in} could be evaluated within a 3x3 window around that point. Hence, only the brightest pixels would be considered. Then, in the attempt to check the surrounding background (to see if the extended object can be a streak rather a star), a new configuration including several small outer windows (12 outer windows in the case of Fig. 11) is more sensitive than the use of a single large outer window. The streak needs to be detected in only one of these windows. The other background pixels do not contribute to diluting the streak statistics. With this filter, the logical conditions to detect a faint star are:

condition 1: $\mu_{in} > 3\,\sigma_n$,

and

condition 2: $\qquad$ max $(\mu_{out-i}) < 2\,\sigma_n$,

where σ_n is the estimation of the local noise standard deviation, μ_{out-i} is the mean signal evaluated for each one of the twelve outer windows and max (μ_{out-i}) is the maximum value of these estimates. Note that the threshold values '$2\sigma_n$' and '$3\sigma_n$' have been set arbitrarily and could be fine tuned but their values are not critical. Also, the signal has already been processed (background removed) and the mean background value is not zero because the pixel values are now only positive integers with values starting at zero. The idea is simply to define a criteria like

$\mu_{out-i} < (\mu_n + tolerance\ factor)$

where μ_n is the average background signal where non-zero values are due to the noise only. The use of σ_n is very practical because it allows the algorithm to adapt to the image noise level. Finally, the inner threshold value has to be higher than the outer threshold value to avoid the situation where a satellite streak is detected in the inner window and not in the outer window; like a star. In such cases, the streak would be systematically erased pixel per pixel by the algorithm. An inner threshold higher than the outer threshold forces the detection of the streak in the outer windows first.

As shown in Table 1, this filter is good at erasing faint stars. It is also good at preserving the streak pixels, even though some faint stars are not erased to ensure preserving that streak. Usually, those undeleted stars are faint enough to create no significant detection with the streak detection algorithm described in Section 3.7.

The main issue occurs when the bright stars have larger profiles. Figure 3 shows that very bright stars, suffering from blooming effects, have larger profiles that may overlap the external windows, which are supposed to only measure the background. In such cases the filter will fail. However, this filter can be adapted to have two or even three passes with different parameters for window size and threshold values. Hence, for bright stars, the inner window size is increased to 11x11 or even 13x13 pixels and the threshold value for the background estimation in the outer window is also increased. Therefore, the detection conditions become something like:

condition 1: $\qquad$ $\mu_{in} \gg 3\,\sigma_n$ $\quad$ (… typically $> 20\,\sigma_n$)

(typically: $\mu_{in} > 1000$ count, i.e. 1% to 2% of the dynamic range of the CCD camera) and

condition 2: $\qquad$ [max $(\mu_{out-i}) < (\mu_{in}\,/\,10)$] or [max $(\mu_{out-i}) < 2\,\sigma_n$].

Hence, the brighter the star in the inner window, the higher the outer window threshold is. When detecting a bright star, this makes the filter less sensitive to background noise.

Table 1. Filter behaviour depending on the cases

Encountered situation	Inner window μ_{in}	Outer windows max ($\mu_{out\text{-}i}$)	result
Faint streak $\mu_{streak} < 3\sigma_n$	undetected	Might be detected	No action, streak is not erased
bright streak $\mu_{streak} > 3\sigma_n$	detected	detected	No action, streak is not erased
Very faint star $\mu_{in} < 3\sigma_n$	undetected	undetected	No action but such a faint signal do not affect the streak detection algorithm
Faint star $\mu_{in} > 3\sigma_n$ and no apparent blooming neither apparent decay	detected	undetected	Requires the execution of the star-removal processing
Bright star $\mu_{in} >> 3\sigma_n$ with apparent decay or blooming	detected	detected	No action: require another filter with larger inner window. The star intensity is an indication of the window size that should be used.
Pair of faint stars	detected	detected	No action: this is the rare case where the filter is eluded.
Star close to a streak	detected	detected	The star is not erased and the streak remains intact.

Bright stars are very easy to detect by nature and the threshold values are not critical. The idea remains that when a bright object is detected in the inner window, one must verify that the brightness is fainter in the outer window to avoid detecting and erasing bright streaks.

In summary, the diagram of Fig. 12 illustrates the entire process proposed to detect and erase stars. It begins with erasing the already known saturated stars that were detected before the removal of the image background (Section 3.4), then by erasing the bright stars and finally by erasing the faint stars. Bright stars are copied and preserved in a separated image for telemetry. Usually, software for calculating the telemetry works better with these clean images where all the artefacts have been removed. Faint stars are simply reset to zero because they are completely confined in the inner window. Bright stars with profiles of various widths are erased using a special process explained in the next section.

7.2 Erasing a star:

There are several methods for erasing a star. There are the bad, the very bad and the appropriate method to do it. All methods are based on the same trick, i.e., when a star is detected, its pixels are set to zero. The main problem is to determine which pixels belong only to the star, which ones are completely outside of its area of influence and

which ones are partially influenced by the star and that may also contain other information (background or near objects). The star profile is unique for each star. It is a combination of optical transfer function plus the degradation produced by the atmospheric transmission and turbulence and the blooming effect. Then, for each bright star, the profile must be measured within the image. Various approaches or combinations of approaches can be used; Fig. 13 illustrates an example where the original image is processed by two different methods giving different results.
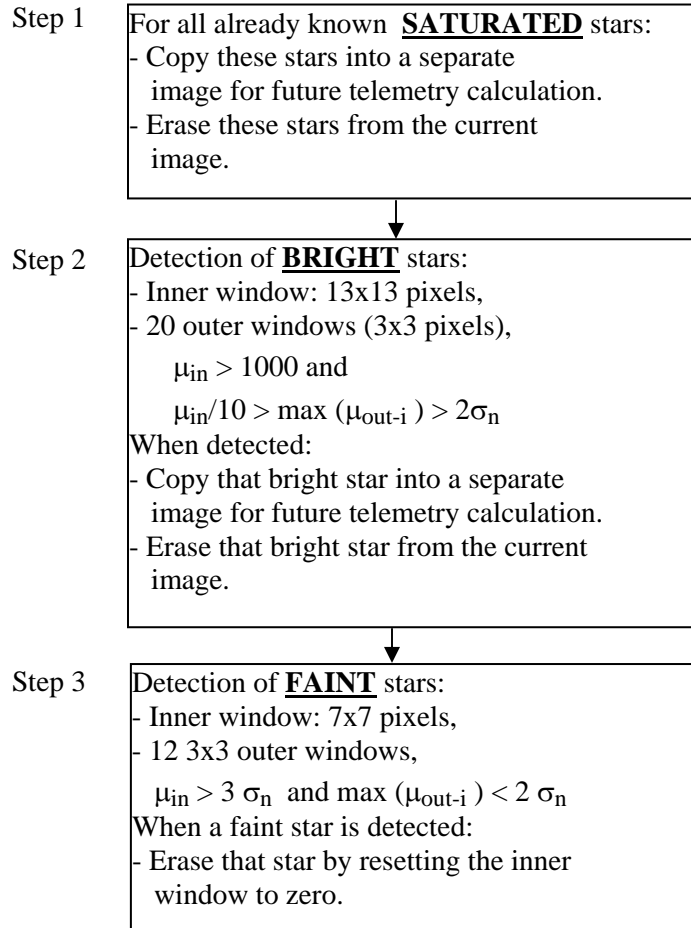
Step 1

For all already known **SATURATED** stars:
- Copy these stars into a separate
  image for future telemetry calculation.
- Erase these stars from the current
  image.

Step 2

Detection of **BRIGHT** stars:
- Inner window: 13x13 pixels,
- 20 outer windows (3x3 pixels),

$\mu_{in} > 1000$ and

$\mu_{in}/10 > \max(\mu_{out-i}) > 2\sigma_n$

When detected:
- Copy that bright star into a separate
  image for future telemetry calculation.
- Erase that bright star from the current
  image.

Step 3

Detection of **FAINT** stars:
- Inner window: 7x7 pixels,
- 12 3x3 outer windows,

$\mu_{in} > 3\sigma_n$ and $\max(\mu_{out-i}) < 2\sigma_n$

When a faint star is detected:
- Erase that star by resetting the inner
  window to zero.

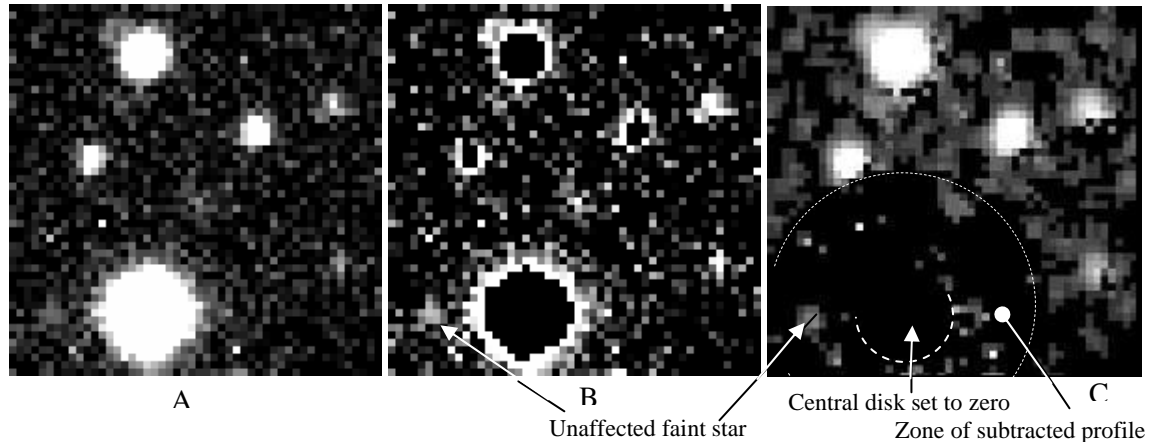*Figure 12.* The three steps of the star detection and erase process

Figure 13. Star removal process: A) an enlarged view of Fig. 19C, B) image where the bright stars have been deleted by setting their bright pixels to zero and C) image where only the brightest star has been erased by setting their central disks to zero and by subtracting their measured profiles over a larger area. This process removes the crown shape artefact that remains in B

The issue is to determine which pixels must be erased. The first method consists in setting the brightest star pixels (above a certain threshold) to zero (as illustrated in Fig. 13B). A better method can be to use a circular mask (of a predetermined radius) where all the pixels contained in this area are reset. In that case, the center of the star is determined by its pixel of maximum intensity and the circular mask is centered on that pixel. This method is very appropriate for faint stars where only a small window needs to be erased. This method is used in step 3 of the diagram in Fig. 12.

However, this method is not appropriate for brighter stars (particularly the saturated ones, such as those considered in steps 1 and 2) where the blooming creates larger star profiles. In those cases, the erasing of the central disk leaves a crown-shape artefact (as illustrated in Fig. 13B). This is not desirable. Larger marks can be used for brighter stars but this solution is not an ideal because very bright stars would require masks so big that large parts of the image would be erased including all the other objects and perhaps the sought streak. Therefore, a clever method is required.

For erasing bright and saturated stars, the selected method combines central mask and peripheral-crown erasing processes. The size of the central circular mask is set to the size of the detection inner window; typically a diameter of 13 pixels (for the 13x13 window of the step 2 of the diagram of Fig. 12). This size can be increased for rare saturated stars, according to the number of saturated pixels, which is an indication of the importance of the blooming and bleeding effects. However, as mentioned previously, excessive bleeding indicates that the image is too corrupted to be of any value for automatic processing.

The peripheral-crown erasing process is a more complicated process because the star profiles $p(r)$ need to be estimated for each star. Then, this profile is subtracted from the image area affected by the star. Here is the process in detail.

The central coordinate (k_o, l_o) of the star is first found (the brightest pixel if sub-pixel accuracy is not required). For all pixels 'I_{kl}' in the area, the radial distance $\left| \vec{r} \right|$ (in pixel unit) is calculated using:

$$\left| \vec{r} \right| = \left| \vec{r}_{kl} - \vec{r}_o \right| = \sqrt{(k - k_o)^2 + (l - l_o)^2} \; .$$

Then, for all pixels 'I' of a similar distance '$\left| \vec{r} \right|$' that form the image subgroup $\in \{I(\left| \vec{r} \right|)\}$, the estimated profile $<p(r)>$ is obtained by calculating the median value of that group of pixels:

$$<p(r)> = \text{median} [\in \{I(\left| \vec{r} \right|) \}].$$

Other operators were tried but the median value was found to be the most robust in the presence of noise and nearby objects. For instance, in Fig. 13-C, a very faint star is included in the area where the bright-star profile is evaluated and subtracted. As one can see this very faint star does not affect the median.

Finally, this profile is subtracted from the image:

$$I'_{kl} = I_{kl} - <p(\left| \vec{r}_{kl} - \vec{r}_o \right|)> \, ,$$

excluding the most central pixels, which are systematically set to zero over the area of the circular mask. Also, $<p(\left| \vec{r}_{kl} - \vec{r}_o \right|)>$ requires a few interpolations of the recorded function $<p(r)>$.

The result is an image where the bright stars disappear without affecting the nearby objects. In fact, there are always artefacts generated by any processing. Fortunately for this case, remaining artefact amplitude is comparable with the background noise level.

The result of the star removal process can be seen in Fig. 19. Figure 19-C shows the image after the gradient background was removed. Figure 19-E shows the same image after removal of the saturated and brightest stars. Finally, Fig. 19-G shows again that same image after removal of (Fig. 12, step 3) all the faint stars. In that last case, the image contrast has been boosted and one can see that only the faint satellite streak remains with a few pairs of closed stars that succeeded to elude the double-gate filters.

7.3   Creation a clean star map

One of the important steps in the image analysis is the determination of the image telemetry. The exact positions of known stars and pixel equivalent celestial coordinates (in right ascension and declination) need to be evaluated. This is done with commercial software that can recognize stars, simply by using rough telescope pointing measurements and a star database. However, this software frequently fails to identify the

stars when the image background is too intense, when there is too much noise or simply when there are too many stars (in this last case, the software cannot converge toward a unique solution).

The performance of such a software package can be improved with a clean star image. When a star is erased from the main image, it is concurrently copied into a parallel image to save telemetry information. By doing so, one generates a clean image without background and with only the optimal number of stars (the brightest ones) required by the telemetry software. The image of Fig. 19-D only shows the brightest stars that were copied into it. This image was processed by the 'CCDSoft' software (created by Bisk Software) and all the stars were recognized. Their magnitudes are listed in Fig. 19-F. With this information available, the real position of the pixel, in terms of right ascension and declination, is known with precision (about one arc second of error). The recognized stars provide information about the image photometry, which can be useful for future analysis of the satellite streak brightness.

8. Streak filtering and detection

The technique for detecting the satellite streak is based on well-known matched filter techniques. However, these methods are usually very sensitive to the background signal and can create several false alarms. This is why the previous filtering process was so critical for the production of an image with a reduced noise and bright star content. Now, one can expect good performance for a matched filter applied to such an enhanced image.

8.1 The a-priori knowledge and the design of the matched filter

To design a matched filter, one must have a priori knowledge (template) of the desired object. This is exactly the case for the current problem. Here the problem is not to detect any kind of satellite streaks but only the streak of the satellite that must be reacquired. This satellite and its orbital parameters are already known. There is only incertitude in its exact current position because of the degeneration of its orbit. This is why it must be periodically re-acquired. Hence, at the moment of image acquisition, the satellite's position can be predicted (using orbital models) at the time at which the camera shutter is opened and at the time at which it is closed, thus providing two positions for two times of reference. These estimated positions should be close to the real satellite positions. They should be inside the telescope field of view (by system design and operation constraints). With this information, the length and orientation of the satellite streak in the image can be estimated. The only remaining unknowns are the real position and the brightness of the satellite. This information will be provided by the convolution peak (the result of the matched filter).

Figure 14 (in the left frame) shows an example of the expected satellite streak. It is in fact modeled by the line segment that links the two expected satellite positions P_1 and P_2 for the two times t and t+dt. This line segment almost corresponds to the matched filter that will be convolved with the image. The matched filter must not inject a phase shift in the solution of the convolution. Therefore, the filter mask must be correctly generated, i.e., the object center must be correctly placed on the window origin (i.e the zero coordinates) such as indicated in Fig. 14. In other words, the object is centered on the top left corner of the window. That filter is also normalized to generate a correlation peak similar in intensity to the object found in the original image. Thus, the amplitude of this generated line segment is 1/n, 'n' being the number of pixels included in that segment.

8.2 The matched filter technique

Figure 15 illustrates the well-known principles of the matched filter technique. The convolution of the image with the filter can be performed by solving the classical double integral for all pixels. This technique is only efficient in terms of processing speed for objects of limited sizes. For long streak (often more than one hundred pixels), it is better to use the global process based on Fourier transform, such as shown in Fig. 15.
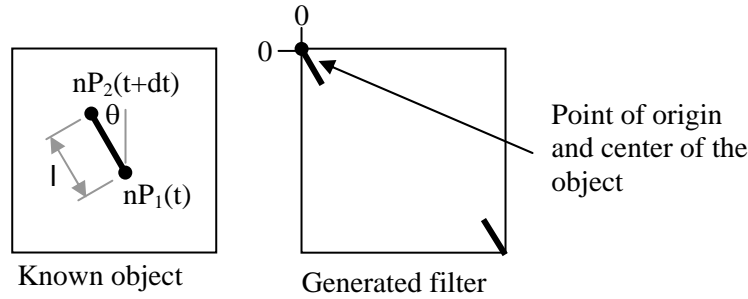
0

$nP_2(t+dt)$

θ

l

$nP_1(t)$

0

Point of origin
and center of the
object

Known object   Generated filter

Figure 14. *Representation of the object and creation of the filter. In the filter, the object is generated from the point of origin in order not to induce a position bias in the response of the convolution*
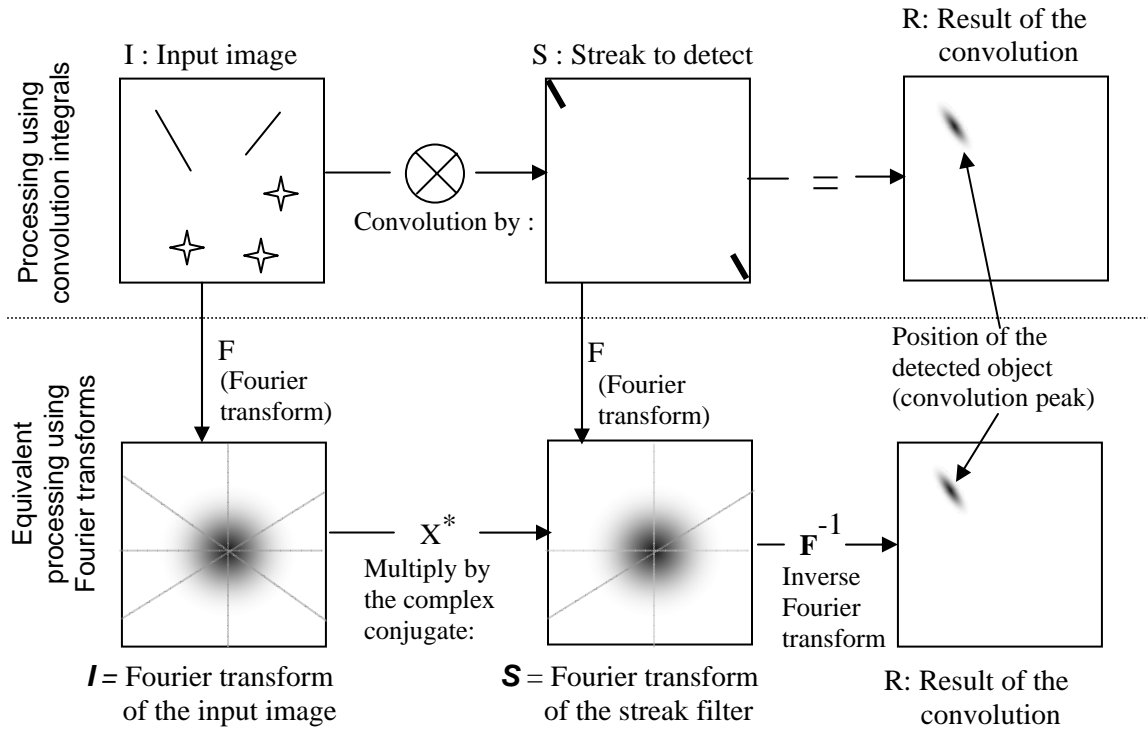
R: Result of the
convolution

I : Input image

S : Streak to detect

Processing using convolution integrals

Convolution by :

=

Position of the
detected object
(convolution peak)

Equivalent processing using Fourier transforms

F
(Fourier
transform)

F
(Fourier
transform)

X^*
Multiply by
the complex
conjugate:

$\mathbf{F}^{-1}$
Inverse
Fourier
transform

$\mathbf{I}$ = Fourier transform
of the input image

$\mathbf{S}$ = Fourier transform
of the streak filter

R: Result of the
convolution

Figure 15. *The convolution peak is obtained by first calculating the Fourier transform for both the image and the filter (or object), by multiplying them (with the complex conjugate) and finally by calculating the inverse* Fourier *transform of the result.*

The Fourier filtering technique is well described in any signal processing textbook. For the benefit of the reader not familiar with that technique, here is a brief description. Let us call the image acquired by the CCD and pre-processed to remove the background and stars 'I', its Fourier transform ($\mathbf{I} = F$ (I)) '$\mathbf{I}$', 'S' the image of the synthesized streak, '$\mathbf{S}$' its Fourier transform ($\mathbf{S} = F$ (S)) and '$\mathbf{S}^*$' its complex conjugate. The convolution of the image with the object is obtained by multiplying their Fourier transforms and then by calculating the inverse Fourier transform of the result, i.e.: $R = F^{-1} \{ \mathbf{I} \ S^*)$. The convolution peak that appears in the filtered image 'R' indicates the location of the searched streak. Figure 19-J shows an example of such a convolution.

8.3 Analysis of the shape of the convolution peak

There may be several false alarms generated by bright objects that do not really match the filter. These objects have so much energy in their structures that even a partial match is still more intense than a perfect match with a faint streak. This is the case of Fig. 19-J where three pairs of relatively bright stars, which survived to the star removal process, generate three convolution peaks more intense than the faint satellite streak. Therefore, the response of the matched filter must be analyzed further to see how the real match can be discriminated from the false alarms. Fortunately, the answer to this problem is quite simple as demonstrate below. Let us see the appearance of the shape of the convolution peak for both objects (streak and star).

When observing Fig. 16, one can see that there is a major difference between the results of the matched-filter for a streak or a star. In theory, the convolved streak has a pyramidal shape with an amplitude 'a' (also the amplitude of the streak in the original image) while a convolved star has almost a rectangular shape (convolved by the narrow star Gaussian profile) with an amplitude of '2b/n', where 'b' is the maximum star intensity and 'n' the streak length in pixel (or the length of the line segment that is used as template). In practice, the result of the filtering method is modulated by noise. Also, the pyramidal shape of the convolution peak may be distorted by the satellite fading (principally due to satellite rotation).
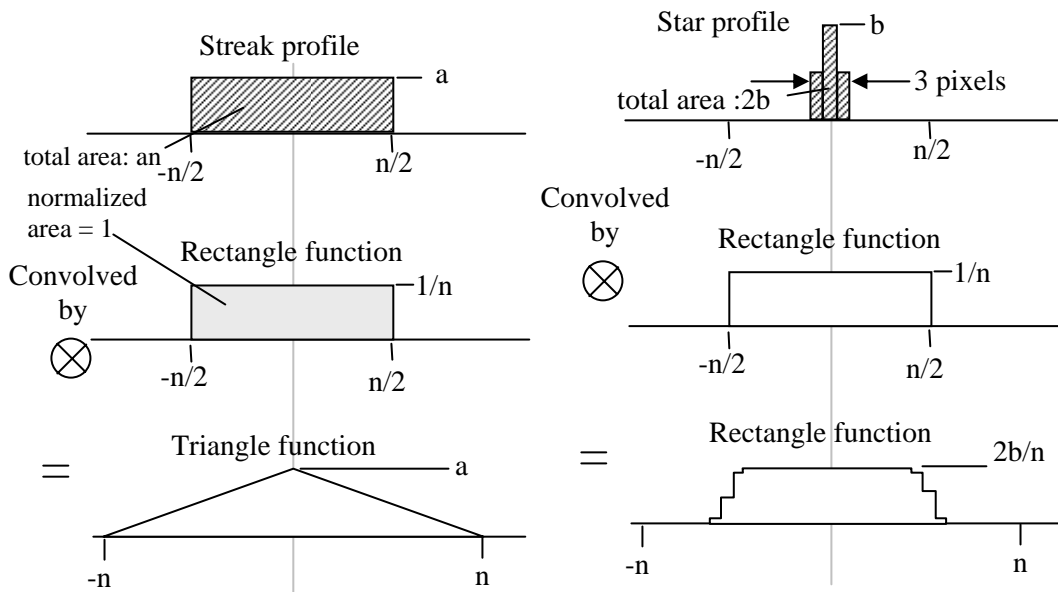
Figure 16. *Matched filter convolution technique: response of a streak and a star when convolved by a 'Rectangle' function*

8.4   Iterative matched-filter technique

This observation is important and suggests what to do in the next processing step. The shape and intensity of the streak convolution peak is similar to the original streak. This is completely different for a star where the convolution peak is a lot fainter than the original star.

This observation suggests the following processing method. For each detected convolution peak, the 'intensity' information can be used to clip the original signal and produce a new enhanced image. In this new image, the original streak is preserved while the stars are attenuated.

Here is the basic principle of the clipping process.   Each object detected, indicated by a convolution peak, is clipped with an adapted 'clipping mask'. The shape of this mask is the streak shape. Its intensity is that of the convolution peak. Therefore, the streak clipping mask is very similar to the real streak. On the other hand, the star clipping masks are larger and fainter than their corresponding stars. The clipping process consists in calculating the minimum between the original image and the clipping masks. Hence, the streak remains unchanged while the stars are severely truncated. Such an enhanced image is shown in Fig. 19 I.

Since the streak remains unchanged after this process, this new enhanced image can be processed again with the matched filter. This will produce a second generation of convolution peaks where the streak convolution peak is unchanged but where the star convolution peak is fainter (Fig. 19 L). This new result can be used to generate the second generation clipping masks and the entire process repeated again and again. Figure 19J and 19L show the convolution peaks after one and three iterations (with the other method described below) while Fig. 19I and 19K show the clip images after as many iterations. Experiments (Ref. 10) showed that 12 iterations produce the best results. There is no visible improvement with additional iterations.

This technique appears very difficult to implement. However, there is a more practical method to achieve the same result.   Rather than searching for every convolution peak and generating several intensity masks, one can simply directly use the previous convolution result. The convolution peaks of the stars already have the appropriate shape (almost a rectangle function such as shown in Figures 16 and 17), location and intensity. Therefore, the convolved image can be used as a global intensity mask, which includes all objects at the same time. This is good for the stars but not for the streak since this is the only object with a triangular-shape convolution peak. However, by multiplying the convolved-image intensity by two, such as shown in Fig. 17, this triangular peak completely contains the streak profile. Figure 21 shows the same thing but with real data. This convolved image (multiplied by 2) can be used as a clipping mask. With this simpler clipping method, the stars are less severely clipped, whereas the streak is entirely preserved.

Figure 17 illustrates the original signal, the shape of the convolution peaks (2x) for the streak and for a star, along with the resulting clipped signal. Figure 18 illustrates the

iterative process that involved all the Fourier transform and signal clipping. As mentioned above, the whole process practically converges after three iterations. After that, the iterative matched filter technique provides no significant improvement. However, an ongoing study (ref. 10) shows that the best SNR is reached after 12 iterations.
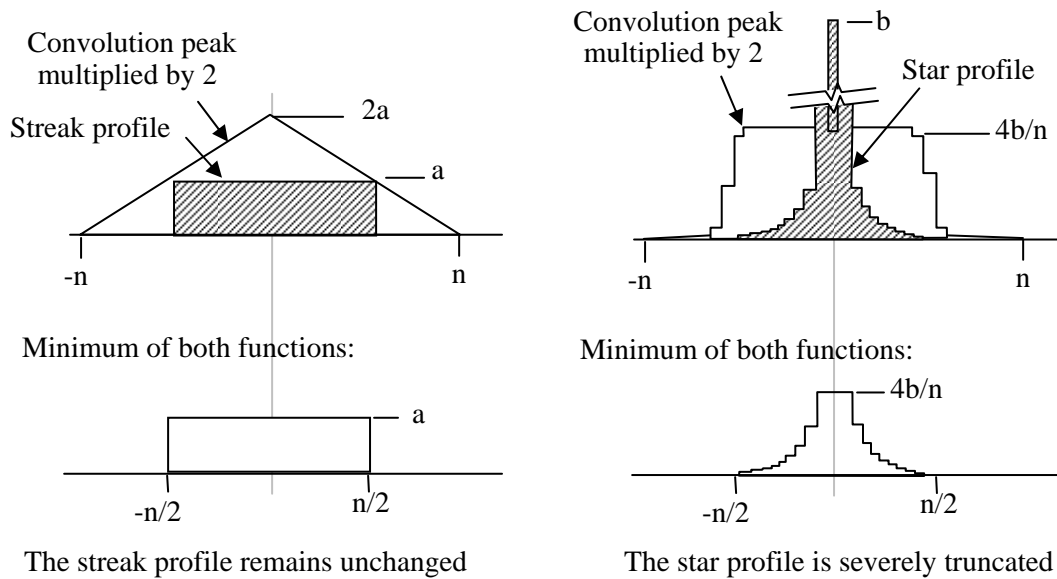

Figure 17. *Clipping the original image using a local intensity threshold function, which is made using the result convolution of the original image with the matched filter.*
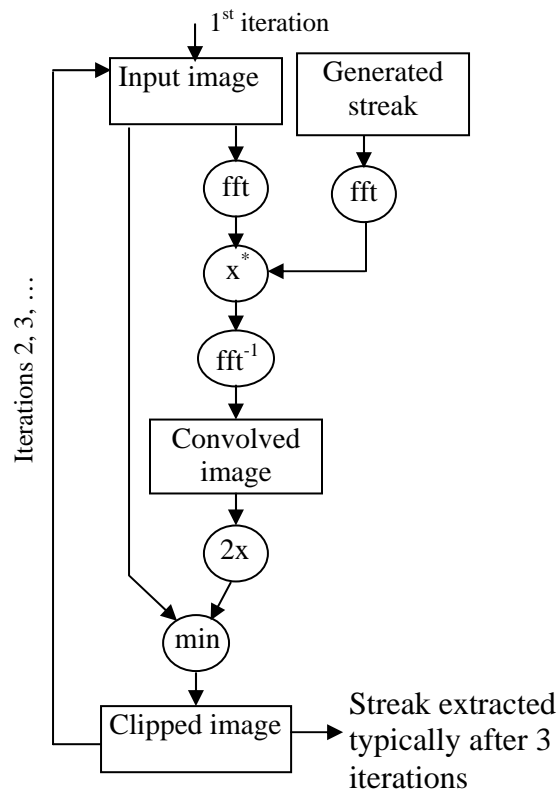
1st iteration

Input image

Generated streak

fft

fft

x*

fft-1

Convolved image

2x

Iterations 2, 3, …

min

Clipped image

Streak extracted typically after 3 iterations

Figure 18. Iterative matched-filter technique

9.   Result

The results of all the processing methods explained above are illustrated in Fig. F19. Starting with the raw image (Fig. 19A), the background is removed (Fig.19C), the stars are erased (Fig. 19G) and the satellite streak is extracted (Fig.19L). The images speak by themselves; this processing is extremely efficient.

The processing methods are very efficient in terms of computer requirements. The first implementation in Matlab was sluggish. However, after once recoded in C++, the complete program was executed in only a few seconds with an old processor (500 MHz). It is even faster to process images than to download them from the CCD camera. Therefore, in this case, the processing time is not a limitation.

Also, the information of the satellite streak is well preserved. Figure 20 shows an enlarged view of the satellite streak 1) after the removal of the background and 2) at the end of the process. Stars close to streak were erased and the noise was almost completely eliminated (particularly by the clipping process during the steps of the iterative matched filtering). Even the star superposed on the streak was attenuated by the clipping process, which improves the perception of the streak. However, the streak was shortened by a few pixels, which indicates that the clipping process (in the iterative matched filter) could be improved. Since the streak signal is close to the noise level (SNR=2 in the present case), the convolution peaks are noisy and so is the clipping mask. However, the profiles showing these thresholds in Fig. 21 seem to indicate that the methods perform as predicted in Fig. 17. The method also seems to be robust to noise.

The methods presented here were tested with success on several images. Not every possible situation has yet been tested, but up to now, detections are not problematic and the algorithm consistently provides good performance. For one of the worst cases where the SNR is only 0.75 (Fig. 4C) and the noise standard deviation is only 3 counts per pixel (i.e., the streak is only 2 or 3 counts above background) the streak was clearly detected. The problem with such a signal is the streak analysis afterwards. Even though it is detected, its telemetry (positions of the end-points, center of mass, etc.) is very uncertain. However, the processing for such analysis requires more elaborate numerical analysis methods, which was not the goal of the present study.
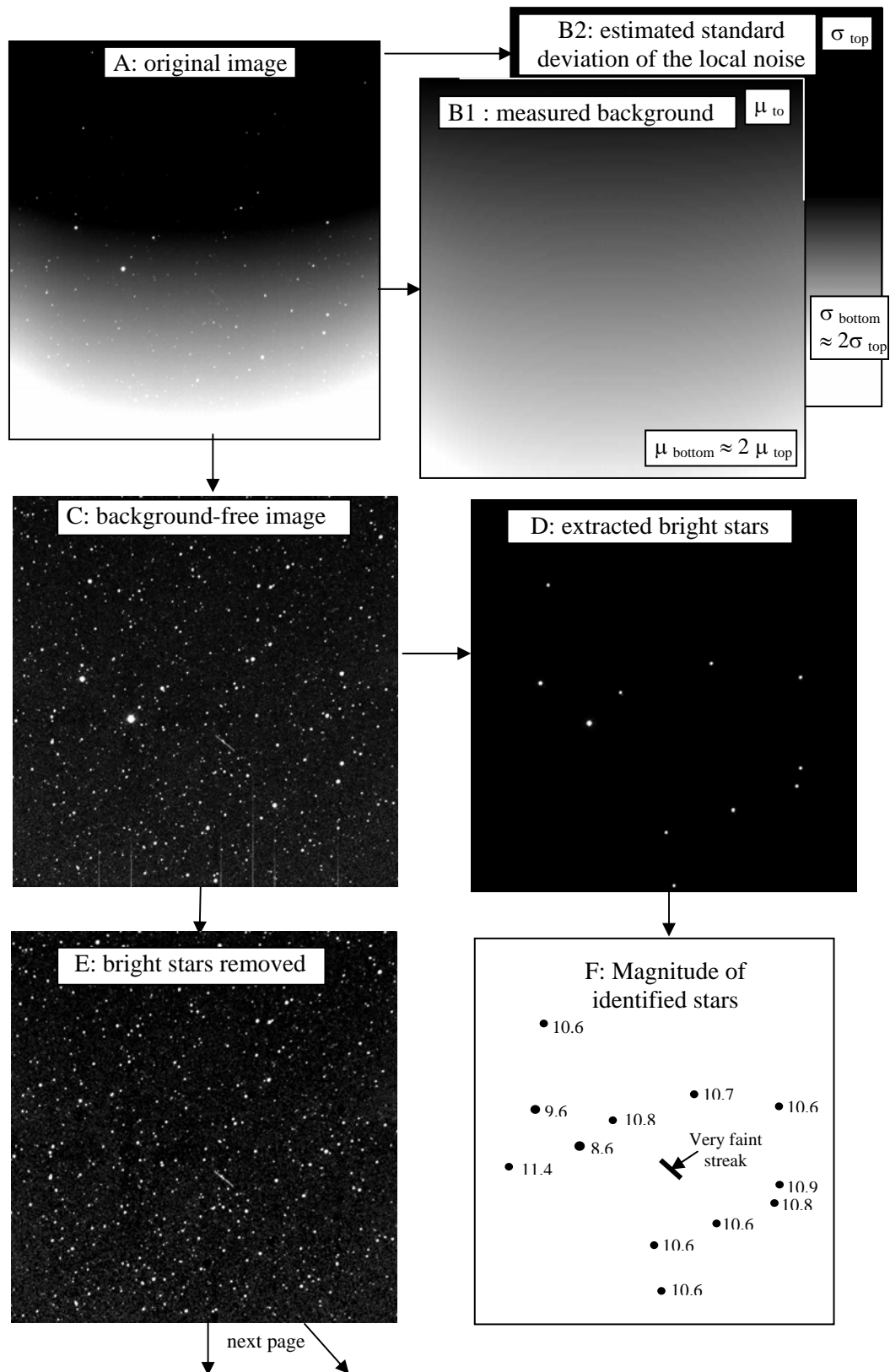
Figure 19. *Evolution of the image through the processing from the raw image to the final detection*
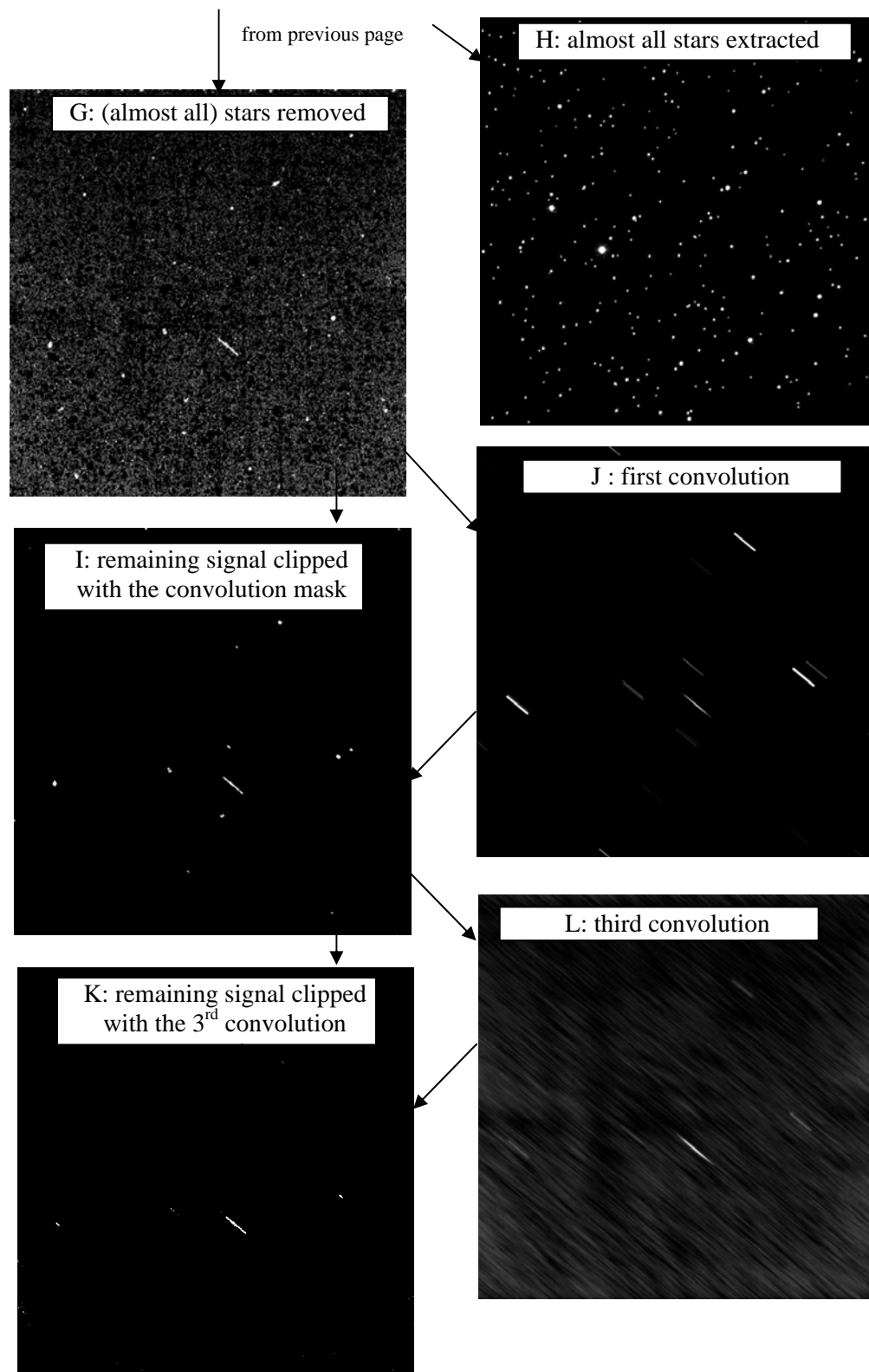
from previous page

G: (almost all) stars removed

H: almost all stars extracted

I: remaining signal clipped with the convolution mask

J : first convolution

K: remaining signal clipped with the 3rd convolution

L: third convolution

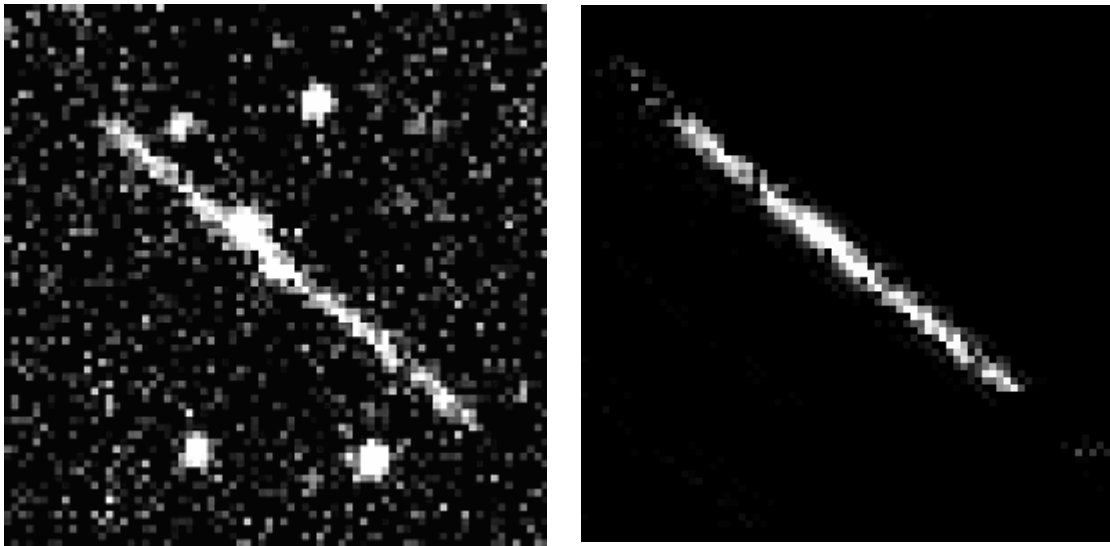**Figure 19 (continue**). *Evolution of the image through the processing from the raw image to the final detection*

Figure 20*. Satellite streak before the matched filter (but with background removed and where the brightest star have also been removed) and that same streak after noise smoothing and three matched-filter iterations.*
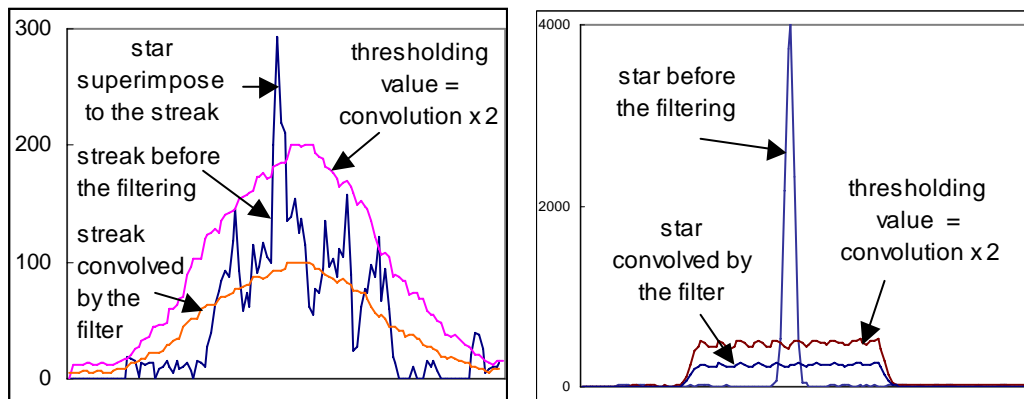

Figure 21. *Profiles extracted from Figs. 19 G and J showing the satellite streak and a star (that survives to the star erasing process) before and after convolution. This figure (like Fig. 17) illustrates with real data how the clipping (achieved through the convolution of the image with the matched filter) preserves the streak but severely truncates the star pixel value.*

10. Future works

The algorithm described previously performs very well. However, there is still room for improvement. For example, some parameters could be adjusted to make the algorithm more robust in the presence of noise. For instance, the threshold mask could be redesigned to better preserve the streak pixels. For example, a bias of σ_n could be added to the threshold technique. This could help to preserve the detected streak and would leave the efficiency of the filter virtually unaffected when a star is to be truncated (as in Fig. 21). However, this requires more experiments that will be made in the next phase of development.

It would be interesting to add post-detection analysis algorithms in order to reject false alarms, validate the detection, extract useful information and generate automatic detection reports. For very faint streaks, the presence of false alarms becomes an issue. Very often, it is obvious that the brightest detection peak is created by one of the remaining bright stars, or more probably by a pair of faint stars that eluded the star erasing process. In those cases, these false alarms could be rejected by performing basic morphological analysis. For example, the shape of a group of pixels (indicated by the brightest detection peak) could be evaluated and if the shape does not correspond to the expected streak shape (as a compact group of pixels created by a star), then this alarm can be discarded and the analysis could continue with the next detected object. Experiments have shown that this kind of situation occurs when the streak SNR is below $2\sigma_n$, where the valid detection is very often the second or third detection peak in intensity. Another interesting post-detection analysis method is the extraction of information about the detected streak. Its length, orientation, position of its geometric center, positions of its end-points, its magnitude, etc. are all information that can validate the detection and allow declaring that the algorithm succeeded or failed. Subsequently, detection reports to this effect can be generated.

_____

Note: At the time, this report is being published, the proposed works in the previous paragraph were undertaken and the results will be published in Ref. 10.

11. Conclusion

The cascade of algorithms described in this document were implemented and tested in Matlab and have proven to perform very well. A more optimized version was developed in C++, which has also proven to be very efficient from the point of view of CPU time. The CPU time, required to process an image for satellite streak detection, is less than 10 seconds. If the sensor is expected to acquire a new observation every three minutes (this is expected for the CASTOR), this is less than the spare CPU time. Therefore, the processing time is not an issue for real time operations. The images can be processed immediately after their acquisition.

The algorithms were implemented in the automatic processing software (at the SOC in DRDC Ottawa) for the operation of the three CASTOR stations. Up to now (after several months of operation and applied to hundreds of images), it has proved to be very efficient and seems to be able to detect everything with a SNR above 2 with almost no false alarms. However, due to the number of pixels in the streak (hundreds of pixels with SNR>2, i.e., the signal is still strong), it is expected that the method can still be improved to detect fainter streaks. For fainter streak intensity, the actual algorithm performance is limited by false alarms (not by the sensitivity) and the suggestion made above (about morphological analysis) may be a solution to lower the detection limits.

Up to now, detections have been achieved with a pixel SNR lower than one. At this level, it is however difficult to extract additional information (like the end-point coordinates) about the streak. Historically, the acquisition and analysis are performed with a human in the loop. One single shot is acquired and the analyst tries to characterize the single streak by measuring its end-points. For very low SNR, end-point cannot be determined with precision and the analyst can only report the observation with inaccurate details. By using numerical analysis, it is possible to extract more reliable information such as the measurement of the geometric center of the streak, which is less sensitive to the noise than the end-point estimation. Furthermore, an automatic system could acquire a strobe streak (with multiple frame expositions), providing several streak segments, which would allow one to calculate several geometric centers and verify whether these detections are coherent. Hence, the processing could increase the sensitivity and reliability of the detection system, but it would require changing the data acquisition procedure. The detection algorithm presented in this document was proven to perform very well. This tool is now being considered for inclusion within the operation tools of the observation stations.

12. References

1. Nishimoto, D.L., et al., "RAVEN: The Evolution of Small Telescopes", 1999 AMOS Technical Conference, Aug.30 – Sept. 3, 1999, pp. 389-394

2. Orth, R., Kervin, P., Nishimito, D., Africano, J., Hamada, K., Law, B., Soo Hoo, V., and Sydney, P., "Raven Operations as a Contributing Sensor in the ITW/AA Network, 2002 AMOS Technical Conference, Sept. 16 – 20, 2002

3. Wallace B., Rody J., Scott R., Pinkney F., Buteau S., Lévesque M. P., "A Canadian Array of Ground-Based Small Optical Sensors for Deep Space Monitoring", 2003 AMOS Technical Conference.

4. Scott R., Wallace B., Pinkney F., Rody J., Lévesque M., Buteau S., Racey T.J., Bennett B., "Metric Accuracy and Limiting Visual Magnitude Analysis of the Canadian Surveillance of Space Concept Demonstrator", 2004 AMOS Technical Conference.

5. Earl, M.A., and Racey, T.J., Progress Report for the Canadian Automated Small Telescope for Orbital Research (CASTOR) Satellite Tracking Facility, Proceedings of the 2000 Space Control Conference, STK-255, MIT Lincoln Laboratory, Lexington, Massachusetts, 11-13 April 2000, pp. 107-114

6. Earl, M.A., and Racey, T.J., The Canadian Automatic Small Telescope for Orbital Research (CASTOR) – A RAVEN System in Canada, 1999 AMOS Technical Conference, Aug.30 – Sept. 3, 1999, pp. 401-410

7. Lelièvre M., Lévesque M. P., Buteau S., 'Measurement of artificial-satellite spectra with a small telescope, DRDC Valcartier TR 2006-141.

8. Buteau S., Lévesque M.P., Bernier A.P., 'Surveillance of space concept demonstrator – Presentation of one sensor: CASTOR-V'. DRDC Valcartier TM 2005-165.

9. Sanders-Reed J. N., "Maximum Likelihood Detection of Unresolved Moving Targets", IEEE Trans. Aerospace and Electronic System, Vol. 34, No. 3, July 1998.

10. Lévesque M. P. and Lelièvre M., 'Improvements of satellite-streak detection by the use of false alarm rejection algorithms', DRDC Valcartier TR 2006-587.

List of symbols/abbreviations/acronyms/initialisms

DND	Department of National Defence
SofS	Surveillance of Space
SOC	Sensor Operation Control
SSOC	Surveillance of Space Operation Center
PSF	Point Spread Function, also called the optical impulse response
SSN	Space Surveillance Network
CASTOR	Former name of the ground stations
SofS/CD	SofS Concept Demonstrator; new name of the ground stations
CCD	Charge Couple Device
SNR	Signal-to-Noise Ratio
ADC	Analog to Digital Converter

Distribution list

1-   Director General

3-   Document Library

1-   M. P. Lévesque (author)

1-   Hd/SOp

1-   Hd/GEO

1-   A. Jouan

1-   M. Levièvre (post-doc student)

1-   J. P Ardouin

1-   D. St-Germain

1-   D. Lavigne

1-   S. Buteau

1-   P. Lahaie

1-   J. Maheu

1-   V. Roy

1-   DRDKIM (PDF file)

1-   DRDC

1-   DRDC Ottawa

1-   DRDC Atlantic

1-   DRDC Suffield

1-   DRDC Toronto

2-   DRDC Ottawa
attn :   B. Wallace,
          R. Scott.

3-   RMC Kinfgston, Dept Physics,
P.O. Box 17000 Stn Forces
Kingston, Ontario, K7K 7B4
Canada
attn: Dr. T. J. Racey,
         Dr. B. Bennett,
         LCdr D. Burrell.

5-   DPDOIS / Surveillance of Space Project (SofSP)
MGen George R. Pearkes Bldg
101 Colonel By Drive, Ottawa, ON, Canada, K1A 0K2
attn: R. D.W. Shelly,
         G. Rumbold,
         Maj. K. D. Johnston,
         Maj. P. B. Boone,
         D. Simmelink.

DOCUMENT CONTROL DATA

1. ORIGINATOR (name and address) DRDC Valcartier, 2456 Boul. Pie XI north, Québec, QC, Canada, G3J 1X5	2. SECURITY CLASSIFICATION (Including special warning terms if applicable) Unclassified

3. TITLE (Its classification should be indicated by the appropriate abbreviation (S, C, R or U)

Image processing technique for automatic detection of satellite streaks

4. AUTHORS (Last name, first name, middle initial. If military, show rank, e.g. Doe, Maj. John E.)

Dr Martin P. Lévesque, Dr Sylvie Buteau

5. DATE OF PUBLICATION (month and year) February 2007	6a. NO. OF PAGES 42	6b .NO. OF REFERENCES 10

7. DESCRIPTIVE NOTES (the category of the document, e.g. technical report, technical note or memorandum. Give the inclusive dates when a specific reporting period is covered.)

Technical report

8. SPONSORING ACTIVITY (name and address)

DRDC Valcartier, 2459 Boul. Pie XI north, Québrc, QC, G3J 1X5

9a. PROJECT OR GRANT NO. (Please specify whether project or grant) WBE: 15et13	9b. CONTRACT NO.
10a. ORIGINATOR'S DOCUMENT NUMBER DRDC Valcartier TR 2005-386	10b. OTHER DOCUMENT NOS N/A

11. DOCUMENT AVAILABILITY (any limitations on further dissemination of the document, other than those imposed by security classification)

- ☒ Unlimited distribution
- ☐ Restricted to contractors in approved countries (specify)
- ☐ Restricted to Canadian contractors (with need-to-know)
- ☐ Restricted to Government (with need-to-know)
- ☐ Restricted to Defense departments
- ☐ Others

12. DOCUMENT ANNOUNCEMENT (any limitation to the bibliographic announcement of this document. This will normally correspond to the Document Availability (11). However, where further distribution (beyond the audience specified in 11) is possible, a wider announcement audience may be selected.)

dcd03e rev.(10-1999)

13. ABSTRACT (a brief and factual summary of the document. It may also appear elsewhere in the body of the document itself. It is highly desirable that the abstract of classified documents be unclassified. Each paragraph of the abstract shall begin with an indication of the security classification of the information in the paragraph (unless the document itself is unclassified) represented as (S), (C), (R), or (U). It is not necessary to include here abstracts in both official languages unless the text is bilingual).

This report presents an image processing technique to detect satellite streaks. This method is particularly useful in the context of surveillance of space where the positions of active satellites and other orbital debris must be monitored. In such cases, the orbital parameters are known, but after a certain time this knowledge deteriorates because of the recent orbit perturbations. Consequently, the satellites need to be re-observed and the orbital parameters must be updated before these satellites are declared lost.

Hence, even before its reacquisition, the satellite's motion is known but its position is estimated with a certain margin of error. This knowledge allows for automatic pointing of the telescope, acquiring of images with the satellite streak within the field of view, developing a matched filter (with the motion knowledge) for detecting this streak within the image and declaring of the satellite position.

This study begins with a detailed analysis of a typical image, which includes several sensor artefacts (such as dead pixels, background gradient, noise) and signal degradation (bleeding, blooming, saturation, etc.). This study explains how sensor artefacts are corrected, image background is removed and noise is partially erased. Then, it describes a technique to detect and erase stars. This reduces the number of objects in the image that could generate false alarms. Finally, this document describes how to design and apply a matched filter used for extracting the satellite streak in images. Examples of processed data are illustrated for each of the processing steps.

14. KEYWORDS, DESCRIPTORS or IDENTIFIERS (technically meaningful terms or short phrases that characterize a document and could be helpful in cataloguing the document. They should be selected so that no security classification is required. Identifiers, such as equipment model designation, trade name, military project code name, geographic location may also be included. If possible keywords should be selected from a published thesaurus, e.g. Thesaurus of Engineering and Scientific Terms (TEST) and that thesaurus-identified. If it is not possible to select indexing terms which are Unclassified, the classification of each should be indicated as with the title.)

Dim target, target detection, background, streak detection, noise reduction, matched filter, image processing, surveillance of space, satellite.

dcd03e rev.(10-1999)

Defence R&D Canada

Canada's Leader in Defence
and National Security
Science and Technology

R & D pour la défense Canada

Chef de file au Canada en matière
de science et de technologie pour
la défense et la sécurité nationale

DEFENCE **R&D** DÉFENSE

WWW.drdc-rddc.gc.ca